MILLIMETER THROUGH VISIBLE FREQUENCY WAVES THROUGH AEROSOLS PARTICLE MODELING, REFLECTIVITY AND ATTENUATION

by

Christos Kontogeorgakis

Thesis submitted to the Faculty of the

Virginia Polytechnic Institute and State University

in partial fulfillment of the requirements for the degree of

MASTER OF SCIENCE

in

Electrical Engineering

APPROVED

Dr. David A. de Wolf, Chairman

Dr. Ioannis M. Besieris

Dr. Charles W. Bostian

May 1997

Blacksburg, Virginia

MILLIMETER THROUGH VISIBLE FREQUENCY
WAVES THROUGH AEROSOLS
PARTICLE MODELING, REFLECTIVITY AND ATTENUATION

by

Christos Kontogeorgakis

Committee Chairman: Dr. David A. de Wolf

Electrical Engineering

(ABSTRACT)

This thesis addresses the problem of modeling atmospheric aerosol (such as haze and fog) particle-size distributions in order to predict the effects (such as attenuation and reflectivity) that these particles have upon the propagation of electromagnetic waves of micrometer range wavelengths. Specifically, an inversely proportional to the fourth power of the particle diameter model is used for haze and the gamma and lognormal distribution models are used for fog. In the case of fog the models are developed based on data consisting of measured fog particle-size distributions at five locations. In this relatively big amount of data, the gamma distribution model is an accurate fit for all the cases and, also, the resulted size distribution does not depend on the altitude. This leads to considerably simpler formulations which yield a linear relationship between the reflectivity factor and the liquid water content. The knowledge of one parameter appears to be enough for defining the model and subsequently predicting reflectivity and attenuation. Attenuation and reflection in haze are found to be insignificant for millimeter wavelengths and somewhat appreciable for the visible ones. In fog, attenuation is found to be extremely high for the infrared-to-visible wavelengths and very low for the millimeter ones.

Acknowledgments

Almost two years ago, when I took the decision to leave my home and country and come for studies in the United States, I didn't know what I was going to find, what exactly I was going to do, whom I was going to work with, and of course what the future would bring about. Now, coming to the end of this course, I realize that I was particularly fortunate to have Professor David A. de Wolf as my advisor for my time in Virginia Tech. He provided me with all the help and support necessary to overcome not only the hardships of the M.Sc. but also the wounds caused by the caprice of life. He showed to me true belief in my work and confidence in my abilities. I owe him most of my academic development, and my maturing as a person. I hope that our paths, both professional and personal, will coincide more than once in the future.

I am also indebted to Dr. Ioannis Besieris. His zeal and devotion in electromagnetics inspired me and offered to me the spark to enlighten my pathway in this field. He always stood by me as a mentor and as a friend.

My sincere gratitude is due to the other member of my thesis committee, Dr. Charles W. Bostian, for providing me the right pointers in writing this thesis.

A part of this work was performed at the *Research Triangle Institute* (RTI). From RTI, many thanks are due to Mr. Rob E. Marshall for his support, help and understanding to the difficulties of that particular time of life.

TABLE OF CONTENTS

LIST OF FIGURES

LIST OF TABLES

1. Introduction

Recent interest in developing technologies [5] to use infrared-to-visible frequency waves propagating in the atmosphere has raised the need to study and, quantitatively, predict the effects of the various weather conditions on these electromagnetic waves. The millimeter wavelengths, already in use and well studied, are very large compared to the diameters of atmospheric particles (Rayleigh regime), and knowledge of the liquid water content suffices in predicting attenuation, reflection, and visibility. Micrometer range wavelengths, though, are not very large compared to atmospheric aerosol particle diameters and thus the more complex Mie scattering calculations must be taken into account as well as the particle size distribution.

Several efforts have been made to estimate attenuation, reflectivity and visibility (see formal definition on page 20) in fog [3,14,26,33] based directly on experimental measurements. This thesis aims to study atmospheric aerosols and more particularly haze and fog, efficiently model the particle size distribution — based on some available collected data — and give quantitative estimations of their effects on the electromagnetic wave propagation.

A purpose of this work is, also, to use the available fog data sets to come up with robust conclusions about the fog particle distribution modeling and test the well-known empirical relationships, which use the liquid water content to predict reflectivity and visibility, to verify them (visibility), or propose new ones when this is not possible (reflectivity).

The gamma function is found to produce a very accurate fit to the available data while the lognormal function seems more suitable when a long size range of particles needs to be modeled. The latter also provides a way to relate the particle size spectrum spread changes with temperature changes.

Attenuation and reflection in haze is negligible for millimeter wavelengths and becomes fairly appreciable for the visible ones. In the case of fog, where the gamma function model is used, attenuation is extremely high for the infrared–to–visible wavelengths, in a very good agreement with experimental results found in the literature. For the K_a (35 GHz) and Q (44 GHz) band (or lower) frequencies attenuation is very low, but it is considerable for the W-band (95 GHz). Visibility is found to range from 50 to 200 m.

The software developed to calculate the above mentioned is listed and described in the Appendix at the end of this thesis.

2. Atmospheric Aerosols

2.1 Introduction and definitions

The atmospheric aerosol is one of the main factors which causes the attenuation of optical waves in the atmosphere and it is also the most variable component of the atmosphere [35]. This variability refers both to its microphysical parameters (such as its number density, size spectrum, complex refractive index, and shape of particles) and to its optical parameters (such as its coefficients of extinction, scattering, and absorption, its scattering phase function, and other components of the scattering phase matrix).

To begin the systematic study of particles, it is first necessary to consider several commonly used definitions of various types of aerosols. Reist [28] defines aerosols as a suspension of solid or liquid particles in a gas, usually air; a colloid. The various types are defined by their chemical composition, size, and shape [28,24] :

Dust : Solids formed by disintegration processes such as crushing, grinding, blasting, and drilling. The particles are small replicas of the parent material, and the particle sizes can range from submicroscopic to microscopic.

Fumes : Solids produced by physicochemical reactions such as combustion, sublimation, or distillation. Typical fumes are the metallurgical fumes of PbO, Fe_2O_3, or ZnO. Particles making up fumes are quite small, below 1 μm in size.

Smoke : A cloud of particles produced by some sort of oxidation process such as burning. Generally, smokes are considered to have an organic origin and typically come from coal, oil, wood, or other carbonaceous fuels. Smoke particles are in the same size range as fume particles.

<u>Mist and Fog</u> : Aerosols produced by the disintegration of liquid or the condensation of vapor. Because liquid droplets are implied, the particles are spherical. They are small enough to appear to float in moderate air currents. When these droplets coalesce to form larger drops of about 100 μm or so, they can then appear as rain.

<u>Haze</u> : Particles with some water vapor incorporated into them or around them, as observed in the atmosphere.

<u>Smog</u> : A combination of smoke and fog, usually containing photochemical reaction products combined with water vapor to produce an irritating aerosol. Smog particle sizes are usually quite small, being somewhat less than 1 μm in diameter

The above mentioned definitions come from popular usage and therefore either overlap or vary. For example, Jaenicke [17] and Mason [23] state that the distinction between aerosols and cloud elements are not well defined, and usually clouds and precipitation are not included as atmospheric aerosols because they consist mainly of water. Those particles, that mainly consist of water, are usually called *hydrometeors* .

Since an aerosol is a collection of particles, it is often desirable [28] to indicate whether the particles are all alike or are dissimilar. Thus there are several other descriptions of aerosols that must also be taken into account.

<u>Monodisperse</u> : All particles exactly the same size. A *monodisperse aerosol* contains particles of only a single size. This condition is very rare in nature.

<u>Polydisperse</u> : Containing particles of more than one size.

Homogeneous : Chemical similarity. A *homogeneous aerosol* is one in which all particles are chemically identical. In an *inhomogeneous aerosol* different particles have different chemical compositions.

Deepak [9], also, distinguishes between the stratospheric and the tropospheric aerosol; The stratospheric aerosol is a well-studied aerosol the broad features of which are, in general, fairly well understood. The tropospheric aerosol, by comparison, is much less well understood, although its immediate impact on human activities can be much greater than that of the stratospheric aerosol. It is the tropospheric aerosol, for example, that is responsible for the hazes that reduce visibility, that affect health factors and esthetic senses, that cause environmental damage, and has the greatest effects on cloud and precipitation processes. Furthermore, depending on the particle production mechanisms and size, the tropospheric aerosol is divided into two main classes [9], continental and marine.

The optical effects of the aerosol are determined [9] by the sizes, optical constants, and shapes of the aerosol. Visibility reduction due to aerosols will be determined mainly by the size distribution and refractive indexes at mid−visible wavelengths. Calculations of other radiative effects, however, such as climatic impact and the effects on infrared transmission, require a more detailed knowledge of the radiative properties of the aerosol, including the absorptive properties of the aerosol at both visible and infrared wavelengths.

2.2 Morphological Properties of Aerosols

2.2.1 Shape

For calculation purposes, it is convenient to think of all aerosol particles as spheres. But, with the exception of small liquid droplets, which are always spherical [28], many shapes are possible. These shapes can be divided into three general classes.

- *Isometric particles* are those for which all three dimensions are roughly the same. Spherical, regular polyhedral, or particles approximating these shapes belong in this class.

- *Platelets* are particles that have two long dimensions and a small third dimension.

- *Fibers* are particles with great length in one dimension compared to much smaller lengths in the other two dimensions.

Particle shape can vary with the formation method and the nature of the parent material. Particles formed by the condensation of vapor molecules are, as mentioned above, generally spherical, especially if they go through a liquid phase during condensation. Particles formed by breaking or grinding larger particles, termed *attrition* [28], are seldom spherical, except in the case where liquid droplets are broken up to form smaller liquid droplets.

2.2.2 Size

Particle size is the most important descriptor for predicting aerosol behavior. Particle diameters of interest in aerosol science cover a range of about four orders of magnitude, from

0.01 μm as lower limit to approximately 100 μm as the upper limit. The lower limit approximates roughly the point where the transition from molecule to particle takes place. Particles much greater than about 100 μm or so do not normally remain suspended in the air for a sufficient length of time to be of much interest in aerosol science. There are occasions where particles that are either smaller or larger than these limits are important, but usually most particle diameters will fall within the limits of 0.01 μm to 100 μm.

Within the range of 0.01 μm to 100 μm lie a number of physical dimensions which have a significant effect on particle properties. For example, the wavelengths of visible light lie in the narrow band of 0.4 to 0.7 μm. Particles smaller than the wavelength of light scatter light in a distinctly different manner than do larger particles.

2.3 Mathematical Representation of Size Distribution

Most aerosols are polydisperse when formed, some more than others. In fact, monodisperse aerosols are very rare in nature [28], and when they do appear, generally they do not last for long.

The simplest way of treating a group of different particle diameters is to use the average or *mean* and the *median* particle diameter. Although each is simple in concept, neither the mean nor the median diameter alone conveys much information about the general range of particle diameters present. Usually more information is required describing the spread of the particle size distribution. The size spectrum of atmospheric aerosols may cover over four decades in radii, namely 10^{-3} to 20 μm [9].

An analytic function generally describes in a smooth way the main features of the aerosol structure. If the size interval of the aerosol diameters is permitted to become very small, since particle counts in most atmospheric suspensions do indicate [10] a continuous size distribution,

the resulting histogram begins to approximate a smooth curve. Then it is possible to represent the distribution by a smooth curve, or better, by some mathematical function, i.e.,

$$dn_i = N(D)dD \qquad (2.1)$$

where dn_i is the number of particles lying in the interval between size (diameter) D and D+dD, and N(D) (m^{-4}) is defined as the number of particles per unit volume (m^3) within a unit diameter range at D measured in m.

Some authors prefer to use a size distribution as a function of radius, namely n(r), which is called *radius-number distribution* [9].

A property of interest is the mode radius r_m for n(r), for which n(r) is maximum, and it is given by the solution of

$$\frac{dn(r)}{dr} = 0 \qquad (2.2)$$

Given some empirical aerosol size distribution data, the problem is to find an analytic function that will most closely represent this data. In the selection of an analytic function to represent the size distribution n(r), according to Deepak [9], the following criteria must be taken into account:

1. The function is not singular for $0 \leq r \leq \infty$;
2. It is easily integrable over r;
3. It can represent the main features of the gross structure of the aerosols by a minimum number of adjustable parameters.

The success of an analytic representation depends upon the selection of an appropriate mathematical function to approximate the actual size distribution data. A model is considered appropriate [9], if properties such as the mode radius, rates of fall-off and polydispersity of the model are similar to that of the experimental size distribution data. This may not always be possible by using a single mathematical function; often a linear sum of mathematical functions may provide a good representation [9]. There seems to be no "special" analytic function that can be said to be unique in representing aerosol size distribution. However, ultimately, it is only when the fitted analytic function leads to results that closely fit the experimental optical (scattering / extinction) data and at the same time falls within the typical physical domain of atmospheric aerosols, that the analytic function may be assumed to represent the aerosol size distribution.

Analytic models suitable for representing aerosol size distributions include the following mathematical functions [9]:

1. Power Law Distribution (PLD)
2. Regularized Power Law Distribution (RPLD)
3. Modified Gamma Distribution (MGD)
4. Inverse Modified Gamma Distribution (IMGD)
5. Lognormal Distribution (LND)
6. Normal Distribution (ND)
7. Generalized Distribution (GD)
8. Power Law Generalized Distribution (PLGD)

More analytically [9] :

1. The Power Law (PL) Model. This model, known as Junge power law, was proposed by Junge to represent his continental aerosol size distribution data and is given by

$$n(r) = p_1 r^{-p_2}, \quad r_1 \le r \le r_2 \tag{2.3}$$

This model becomes singular at r=0, if r_1=0. Even though this model may not always represent a real situation, and does not meet the selection criteria, it is popularly used as it readily gives analytically tractable results.

2. The Regularized Power Law (RPL) Model. In order to eliminate the singularity at r=0 that occurs in Model 1, but maintaining an approximate power law behavior at larger r, one may use a regularized form of the power law,

$$n(r) = \frac{p_1}{p_2} \frac{\left(r / p_2\right)^{p_3-1}}{\left[1 + \left(r / p_2\right)^{p_3}\right]^{p_4}} \tag{2.4}$$

The parameter p_2 controls the mode radius, being a multiplicative factor, while p_3 and p_4 control the positive and negative gradients, and hence polydispersity. The parameter p_3 controls the positive gradient while both p_3 and p_4 influence the negative gradient.

3. Modified Gamma Distribution (MGD) Model. Deirmendjian [10] has shown that this function can be used to describe various types of realistic aerosol distributions.

The radius-number distribution is given by

$$n(r) = p_1 r^{p_2} \exp(-p_3 r^{p_4}) \tag{2.5}$$

The parameter p_3 has the main effect on mode radius and the parameters p_2 and p_4 control the polydispersity. The parameter p_2 determines the limiting behavior as r→0 while the parameter p_4 determines the limiting behavior as r→∞.

4. Inverse Modified Gamma Distribution. This distribution has the same form as Model 3 except that the inverse radius is used. This results in an exponential fall-off at the small size end and power law behavior at the large-radius end. This form of the modified gamma distribution is suggested for dry aerosols.

The radius-number distribution is given by

$$n(r) = p_1 \exp(-p_3 / r^{p_4}) / r^{p_2} \tag{2.6}$$

The parameters p_2 and p_4 control the rate of fall-off at large and small radii, respectively, and hence control the polydispersity. The parameter p_3 controls the mode radius.

5. The Lognormal Distribution (LND) Model. The lognormal distribution generally provides a better description of particle size distribution than the normal distribution because particle sizes, like many naturally occurring populations, are often asymmetric. In this distribution it is ln(r) rather than r which is normally distributed.

The radius−number distribution is given by

$$n(r) = \frac{p_1}{\sqrt{2\pi} p_3 r} \exp\left[-\frac{1}{2} \left(\frac{\ln r - \ln p_2}{p_3} \right)^2 \right] \tag{2.7}$$

The parameter p_3 controls the polydispersity of the model and the parameter p_2 has a multiplicative effect on mode radius.

6. The Normal Distribution (ND). The normal distribution is a symmetric distribution which is finite at r=0 and, thus, strictly speaking cannot be used to represent aerosol size distributions at small r. It can be used to represent size distributions at other ranges of r, and since it is a Gaussian distribution, which has well known properties, such a model can be very useful in certain applications. It is given by

$$n(r) = \frac{p_1}{\sqrt{2\pi}p_3} \exp\left[-\frac{1}{2}\left(\frac{r - p_2}{p_3}\right)^2\right]$$
(2.8)

In the normal distribution, the parameter p_2 controls the mode radius and the parameter p_3 controls the polydispersity.

7. The Generalized Distribution Function (GDF). This distribution is finite at r=0 and, thus does not, strictly speaking, represent particle size distributions at small r. However, it is a versatile function with a wide variety of applications, including altitude distributions, and is therefore included here as a potential representation of aerosol size distributions.
The radius number distribution is given by

$$n(r) = \frac{p_1(1 + p_2)^2 \exp(r/p_3)}{[p_2 + \exp(r/p_3)]^2}$$
(2.9)

The parameter p_3 can be considered as a scale radius and the parameter p_2 determines the type of the function. For $p_2=0$ the distribution becomes an exponential, and for small p_2 the function initially falls off more slowly than the exponential. As the parameter p_3 increases, the spread or polydispersity of the function increases.

8. Power Law Generalized Distribution Function (PLGDF). This model is a versatile function which is most useful when the data to be fitted have broad peaks.

The radius number distribution is given by

$$n(r) = \frac{p_1 \exp\left(p_2 / r^{p_4}\right)}{r^{p_4+1}\left\{1 + p_3\left[\exp\left(p_2 r^{p_4}\right) - 1\right]\right\}^2} \qquad (2.10)$$

The parameter p_2 controls the rate of fall-off at small radii while the parameter p_4 controls the rate of fall-off at large radii. The parameter p_3 controls the spread of the distribution, the breadth of the peaks increasing with large values of p_3.

3. EM Wave – particle interaction

When a particle is illuminated by an electromagnetic beam, that particle can remove energy from the beam (absorption) and convert it to other forms of energy (e.g. heat) or scatter energy to different directions (scattering). In the case of particles in a collection, such as atmospheric particles, each particle is excited by the external field and the resultant field scattered by all the other particles. If we assume [4] that the number of particles is sufficiently small and their separation sufficiently large such that, in the neighborhood of any particle, the total field scattered by all the particles is small compared with the external field, then the total scattered field is the sum of the fields scattered by the individual particles (single scattering). There are no precise general conditions, found in the literature, under which the above assumption is satisfied other than density considerations. For example, in clouds multiple scattering can be appreciable [4].

When there is no systematic relationship between the phases of the waves scattered by the individual particles (out-of-phase) the scattering is called *incoherent*. An unchanging phase relationship gives rise to *coherent* scattering. However [4], in a collection of randomly separated particles, the scattering is always coherent in the forward direction. The scattered energy which is out-of-phase with the original incident beam tends to interfere destructively on average but its own contribution to attenuation is usually negligible [7]. This incoherent scattered energy therefore is not important for the overall mean attenuation but it can be important in disrupting communication signals (e.g. fading) [22].

At a distance of many wavelengths from the source, an electromagnetic wave can be viewed as a plane wave consisting of an electric field, with amplitude E, and a magnetic field, with amplitude $H=(\varepsilon/\mu)^{1/2}E$, perpendicular to each other and both perpendicular to the direction of propagation. The product represents the power flux and it is proportional to $|E|^2$ and, therefore, the electric field suffices for power calculations [22]. For calculation purposes, the sensor signals

are practically monochromatic and one may work with the electric field expressions for plane monochromatic waves of arbitrary polarization. Additionally, the atmospheric particles involved in this work (haze / fog), as mentioned earlier, can be treated as dielectric spheres.

3.1 Attenuation

Attenuation calculations are based on the concept of coherent scattering as well as absorption. A fraction of the original energy (decreasing with distance) undergoes many scatterings with practically no change in direction and therefore remains in phase; this, together with the unscattered energy constitute the coherent energy. It decays exponentially in a uniform medium. The result of the theory [22] is that the electromagnetic power flux at z can be written as exponentials of path integrals modifying the input power:

$$P(z) = P(0)e^{-2S_i}, \quad S_i = \int_0^z d\zeta \left[\alpha_{ab}(\zeta) + \alpha_{sc}(\zeta) \right] \tag{3.1}$$

This expression holds for a simple plane wave. Some modifications are needed if the propagation distance z is so large that spherical spreading of the beam must be accounted for. Likewise, the two α's (amplitude absorption and scattering coefficients) may be integrals over directions perpendicular to z to account for inhomogeneities in those directions. We shall not distinguish between the two α's so that only a sum-α representing overall attenuation will be considered. The exponential decay factor is [35,30] :

$$S_i = \frac{2\pi}{k} \int_L dz \int_0^\infty dD n(z,D) f(k,D,\varepsilon) \tag{3.2}$$

for a path length L, wavenumber k, particle-size distribution n(z,D) in terms of diameter D and altitude z, and particle attenuation factor $f(k,D,\varepsilon)$ (imaginary part) which describes the effect of a

particle on a plane monochromatic wave without changing its direction (the "forward-scattering" amplitude).

If the diameter D is much smaller than the wavelength λ (Rayleigh regime), then the forward scattering amplitude, for dielectric spheres, is approximated by [19] :

$$f_{fs}(k,D,\varepsilon) = f_{bs}(k,D,\varepsilon) = \frac{\pi^2}{2\lambda^2}\frac{\varepsilon_r - 1}{\varepsilon_r + 2}D^3 \tag{3.3}$$

while, if the diameter is comparable to the wavelength, the more complex Mie [4,25,16] scattering calculations have to be used.

3.2 Reflection

In considering the reflection from atmospheric particles, it is helpful to regard the signal as if it were a pulsed one with width in time. The particles may be regarded as incoherent reflectors, i.e. powers reflected from each particle may be added. The reflected signal at any time can be shown to be due to a region of length ≈ cτ/2 at some depth in the haze medium. The reflected power from this region is represented in terms of a cross section q(z), which is a ratio of reflected power to incident flux and therefore has a dimension of an area (and is independent of beam spread and distance from the source). For a depth z into the medium, a simple expression would be,

$$P_{refl}(z) = q(z)e^{-4\int_0^z d\zeta \alpha(\zeta)}S_o(z) \tag{3.4}$$

given that $S_o(z)$ is the incident electromagnetic flux at a location in the absence of the medium. The exponential factor takes into account the attenuation in power on the way in and on the return path to the source. Ordinarily, $q(z)$ contains a volume factor $\approx (c\tau/2) \times (z\theta)^2$ determined [16] by the range cell (which is laterally bounded by the angular extent θ of the beam). This information is embedded in the reflected signal in some other fashion if CW signals instead of pulses are used. We shall give $q(z)$ per unit volume, i.e. in m^2/m^3, so that the user of these results can insert whatever range cell or equivalent volume measure is desired.

Reflection from spherical particles can be handled reasonably well by analytical means, if one includes the numerical evaluation of Mie series [4,25]. However, for small particles (Rayleigh-regime), the backscatter cross section from a dielectric sphere, using (3.3), is [19]:

$$\sigma_{bs}(k,D,\varepsilon) = \left| f_{bs}(k,D,\varepsilon) \right|^2 = \frac{\pi^5}{\lambda^4} \left| \frac{\varepsilon_r - 1}{\varepsilon_r + 2} \right|^2 D^6 \tag{3.5}$$

The reflection from a unit volume of particles, all of which are small with respect to the wavelength and all of which scatter incoherently (i.e. individual scattered powers add up), yields an effective backscatter cross section,

$$q = \int_{D_{\min}}^{D_{\max}} dD n(D) \sigma_{bs}(k,D,\varepsilon) \tag{3.6}$$

Note that the dimension of q is in $m^2/m^3 = m^{-1}$ and that q is a function of k and ε. If the reflection is sensed by a pulse of time width τ, then q needs to be multiplied by half the pulse volume, i.e. by $0.5c\tau\,(L\theta)^2$ and the result is a cross section in the familiar m^2 units.

-17-

3.3 Liquid Water Content and Radar Reflectivity Factor

A quantity widely used, due to measuring convenience, in predicting attenuation, reflectivity and visibility [1,26,3,31] is the liquid water content.

The liquid water content (M) is the total water mass per unit volume of the droplets. It is usually expressed in g/m^3 and analytically, for a collection of spherical water drops with size distribution n(D), given by

$$M = \frac{\pi}{6}\rho_w \int_0^\infty dD D^3 n(D) \tag{3.7}$$

where ρ_w is the specific mass of water ($\approx 10^6$ g/m^3).

For particles very small compared to the wavelength, according to the equations (3.2), (3.3) and (3.7), the attenuation coefficient is given by :

$$S_i(z) = \frac{6\pi}{\lambda \rho_w} \mathrm{Im}\left[\frac{\varepsilon_r - 1}{\varepsilon_r + 2}\right] M(z) \tag{3.8}$$

which predicts that the attenuation coefficient to water content ratio is independent of altitude.

In the same context (Rayleigh regime), equations (3.5) and (3.6) give :

$$q = \frac{\pi^5}{\lambda^4}\left|\frac{\varepsilon_r - 1}{\varepsilon_r + 2}\right|^2 Z, \quad \text{with} \quad Z \equiv \int dD D^6 n(D) \tag{3.9}$$

The factor Z (in mm^6/m^3), or $10\log_{10}Z$ (in dBZ), is called *radar reflectivity factor* and is widely used [1,26,12] to characterize the region responsible for the backscatter since the other factors in (3.9) are presumably known (λ is the radar wavelength, and ε is the relative permittivity of the particles of the medium). The expression (3.9) emphasizes the importance of the larger particles which weight the integrand by the sixth power of the diameter.

The wavelengths used traditionally in radar engineering (in the order of at least a few millimeters) are much larger than the atmospheric particles and therefore the Rayleigh approximations can be used and the use of (3.9) is justified. Nevertheless, when shorter wavelengths are to be employed (such as visible, or infrared / lidar), then the more accurate Mie backscatter cross section should be used in (3.6). In this case, it is inferred from (3.6) and (3.9) that the reflectivity factor Z is more properly given by

$$Z = \frac{\lambda^4}{\pi^5}\left|\frac{\varepsilon_r + 2}{\varepsilon_r - 1}\right|^2 q = \frac{\lambda^4}{\pi^5}\left|\frac{\varepsilon_r + 2}{\varepsilon_r - 1}\right|^2 \int dD n(D)\sigma_{bs}(k,D,\varepsilon) \qquad (3.10)$$

and, unlike the Rayleigh regime case, Z is now a function also of the wavelength λ and the permittivity ε.

Alternative expressions for Z(z) and M(z) in the Rayleigh regime are [8,26],

$$Z(z) = \left(\frac{6}{\pi}\right)^2 n_3(z)\langle v^2(z)\rangle, \quad \text{and} \quad M(z) = \rho_w n_3(z)\langle v(z)\rangle \qquad (3.11)$$

where $n_3(z)$ is the particle density (in m^{-3}), and $\langle v^n(z)\rangle$ is the nth moment of the particle volume $\pi D^3/6$ [i.e. the sum of all particle volumes per unit air volume weighted by n(D) and divided by $n_3(z)$]. From (3.11) it follows that,

$$Z(z) = \left(\frac{6}{\pi}\right)^2 \frac{\langle v^2(z) \rangle}{\langle v(z) \rangle} \frac{1}{\rho_w} M(z)$$ (3.12)

This expresses a linear relationship between Z and M.

Other than the analytical forms for Z, there are several empirical law relationships that have been proposed [1,26] to associate radar reflectivity in fog with liquid water content. A common one proposed by Atlas [1] is:

$$Z = 0.048 M^2$$ (3.13)

where Z is in [mm^6 m^{-3}], and M the liquid water content [g m^{-3}].

3.4 Visibility

An "object" is "visible" when the contrast to its background is high enough. The contrast [13] decreases with distance with the same rate as the intensity of the light

$$C = C(0)e^{-bs}$$ (3.14)

where b is the power extinction coefficient [m^{-1}] and s is the distance [m] from the object.

The visibility is defined as the distance at which the test object is just distinguishable from the background. Hence we need to define a minimum contrast that the eye can distinguish and this, based on observation, is 2% or

$$\frac{C}{C(0)} = 0.02 \Rightarrow e^{-bs^*} = 0.02 \Rightarrow s^* = -\frac{\ln 0.02}{b} = \frac{3.912}{b} \qquad (3.15)$$

where s^* is the visual range corresponding to the visibility.

It is obvious that, in terms of visibility, the extinction coefficient is calculated for a wavelength within the visible spectrum and, therefore, the Rayleigh approximations do not hold.

Besides the above definition for visibility there are empirical formulas to calculate or better predict it [3,20], based on the liquid water content. For advection fog, Koester and Kosowsky give :

$$V = 0.02381M^{-0.64935} \qquad (3.16)$$

where V is the visibility in km and M is the liquid water content in g m^{-3}.

4. Experimental Data Analysis and Distribution Modeling

4.1 The data

The fog data sets, provided Zak [34], were obtained at five different locations - Vandenberg AFB, CA (VAN), Arcata, CA (ARC), Worcester, MA (WOR), Huntington, WV (HUN), and Santa Maria, CA (SM) - during flight tests. An aircraft made several landings in 10 minute intervals, at these sites, along a three degree glideslope measuring particle size distribution, liquid water content and temperature at each ten meters in the vertical. The size distribution was measured in number of drops in "bins" of 3 μm spreads in drop diameter from 2 to 47 μm. For some sites data for larger drops were obtained in 20 μm (VAN,ARC) and 300 μm (WOR,HUN,SM) bins for diameters up to 310 μm and 4650 μm respectively. These larger drop measurements, however, were taken by using different instrumentation which is designed to detect precipitation (i.e. drizzle, rain) [34].

It is important to notice that the data exhibit large variations from approach to approach, and it appears that zero is registered for the smaller particle range, when the number of drops is less than 10^4. This inaccuracy has a very small effect on the total number of particles, leading to an underestimation of 0-2%. However, it is not that this effect itself that can lead to false results, but it indicates that are possibly other unknown errors in the measurements which affect mostly the larger particle data where the numbers are very small. There are some "data correction" methods developed [26], based on the knowledge of the measuring instrumentation, to improve the accuracy of the measurements, yet leading either to considerable underestimation or overestimation of the actual water content (because they mainly affect the larger particle concentration).

For these reasons and because theoretically particles with diameter larger than 100 μm constitute precipitation rather than fog drops, only the 2-47 μm range of the data are used in the calculations for fog. Also, we can assume that atmospheric conditions remain practically the same during the measurements because the time interval between the runs is small enough. Hence, the first step of the data analysis is to average the number of drops for each bin over the total number of landings (approaches). It is obvious that the more approaches are taken, the more reliable are the data. In this context VAN, and ARC, are chosen to be mostly used in the calculations and as the most reliable source to draw conclusions.

Figure 1 to Figure 5 show a 3-D profile of the average fog data for the five data sets available. It can be observed that even the average data have strong variations, especially with altitude.
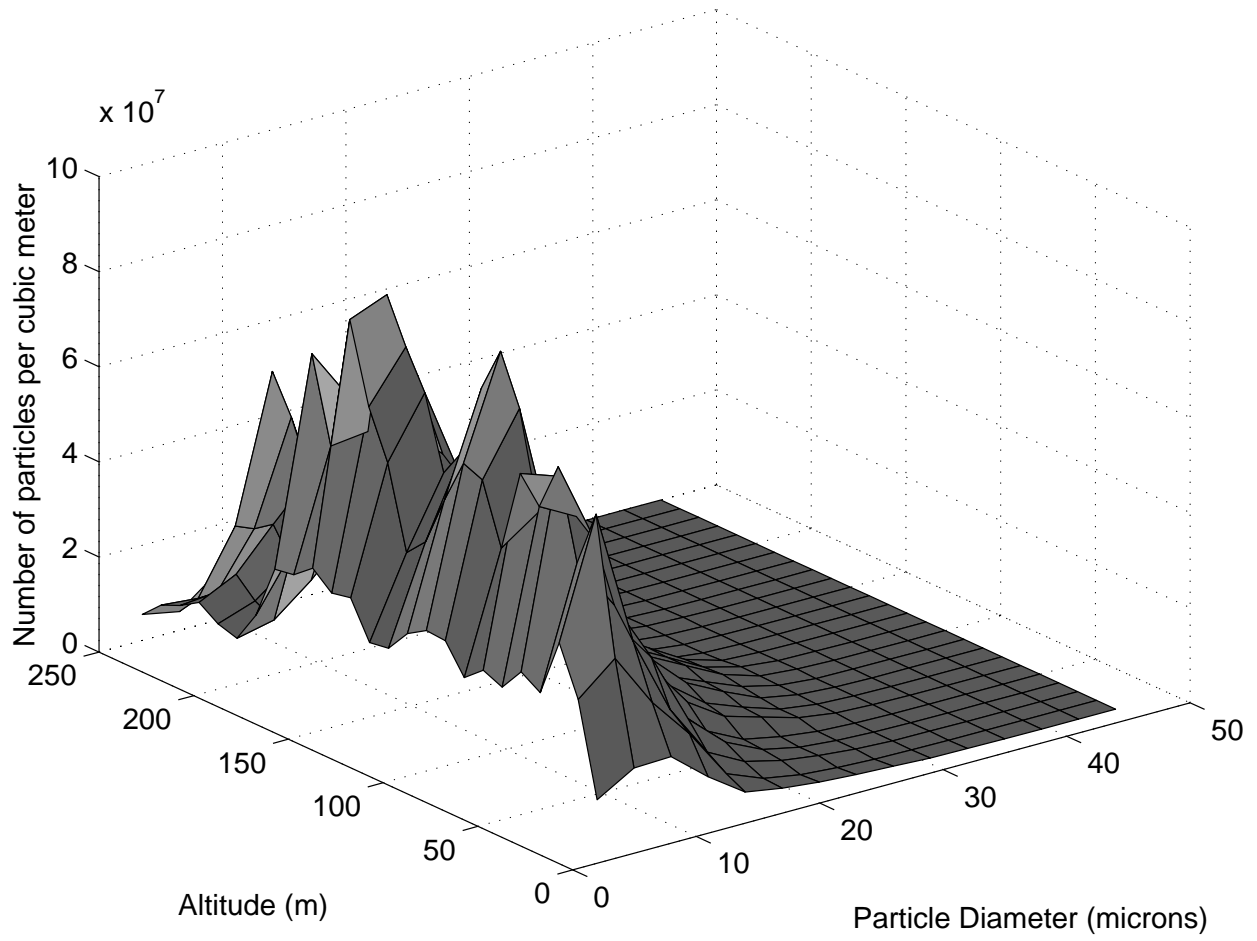
Figure 1. 3-D profile of the average fog data for Vandenberg.
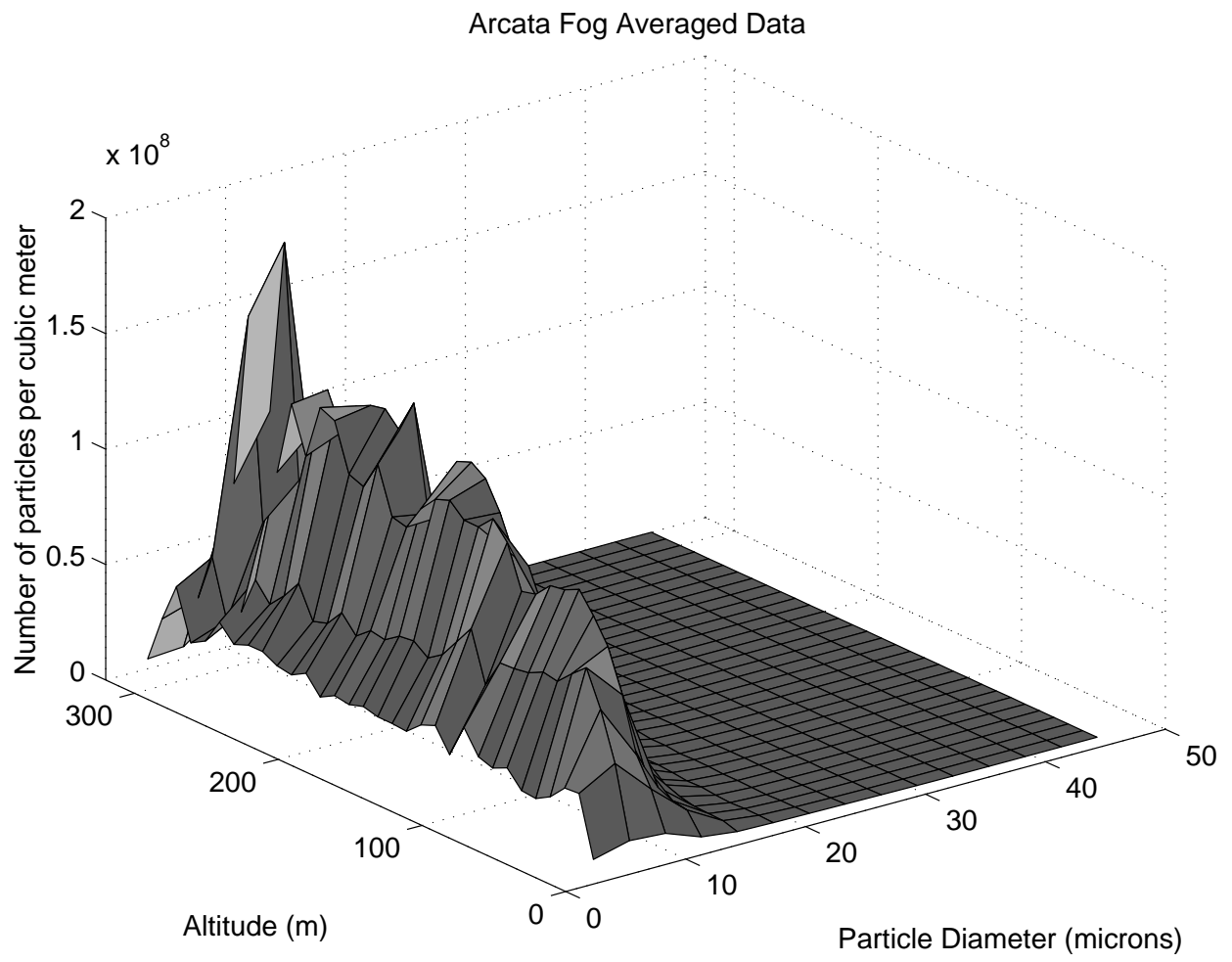
Figure 2. 3-D profile of the average fog data for Arcata.
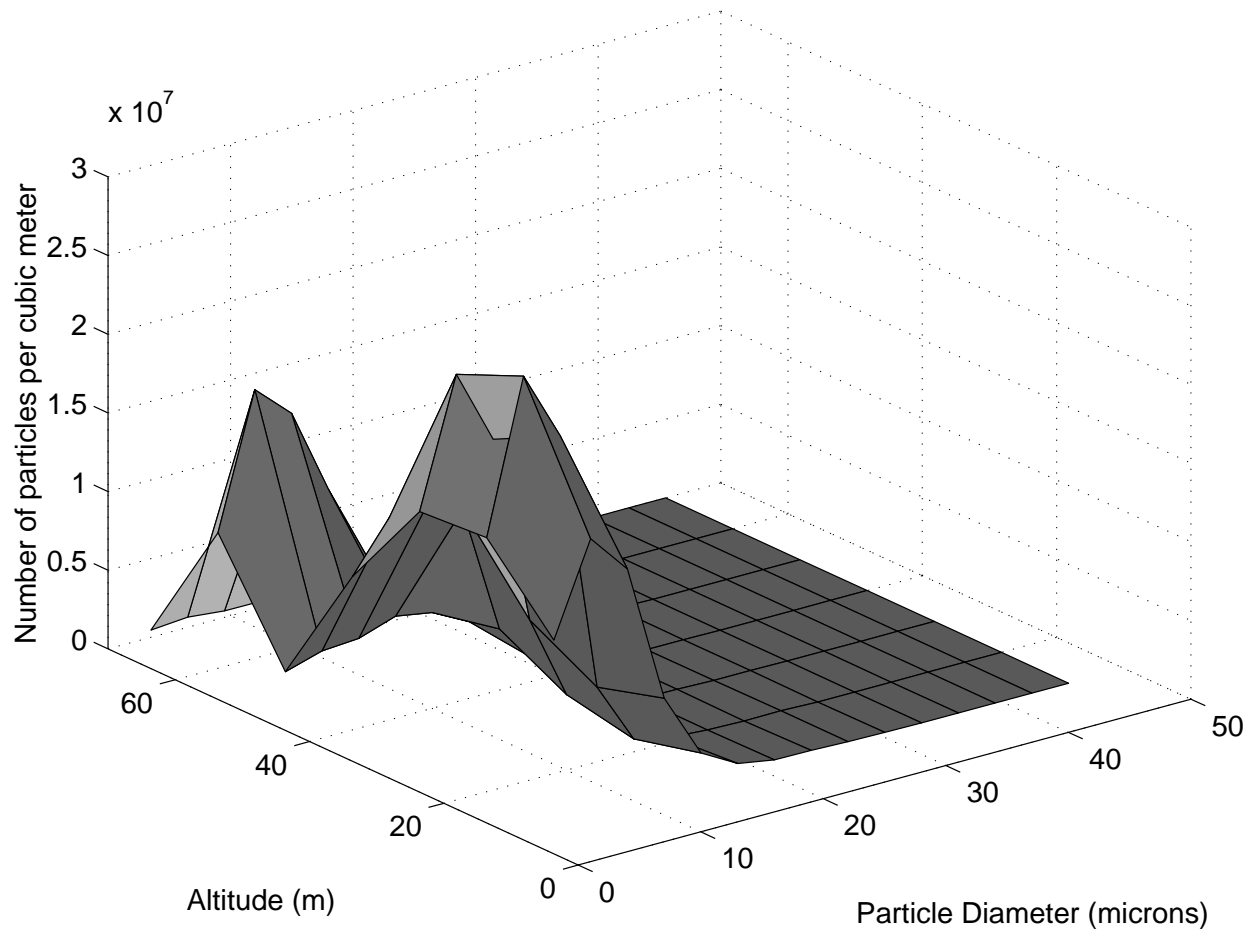
Figure 3. 3-D profile of the average fog data for Huntington.
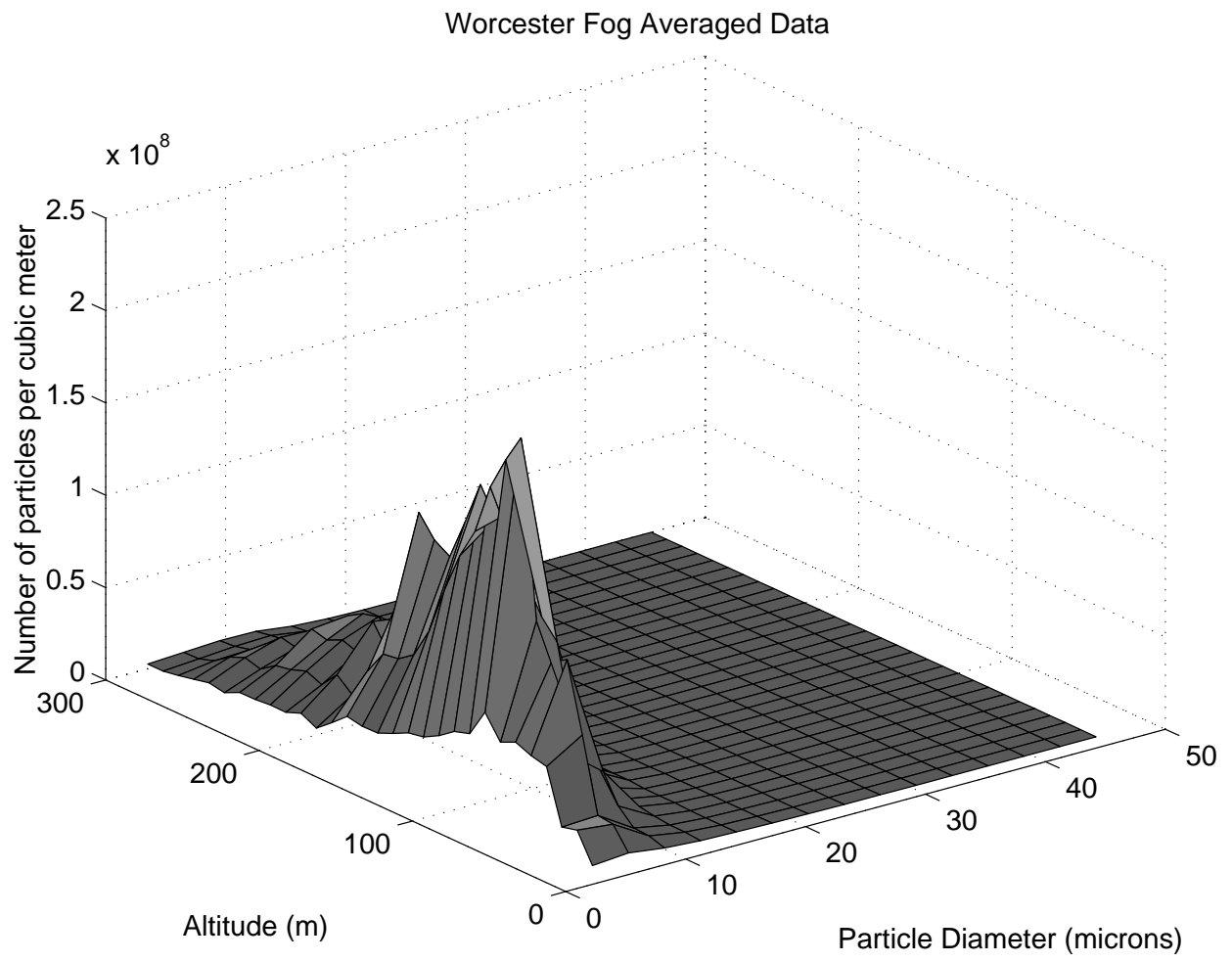
Figure 4. 3-D profile of the average fog data for Worcester.

Figure 5. 3-D profile of the average fog data for Santa Maria.
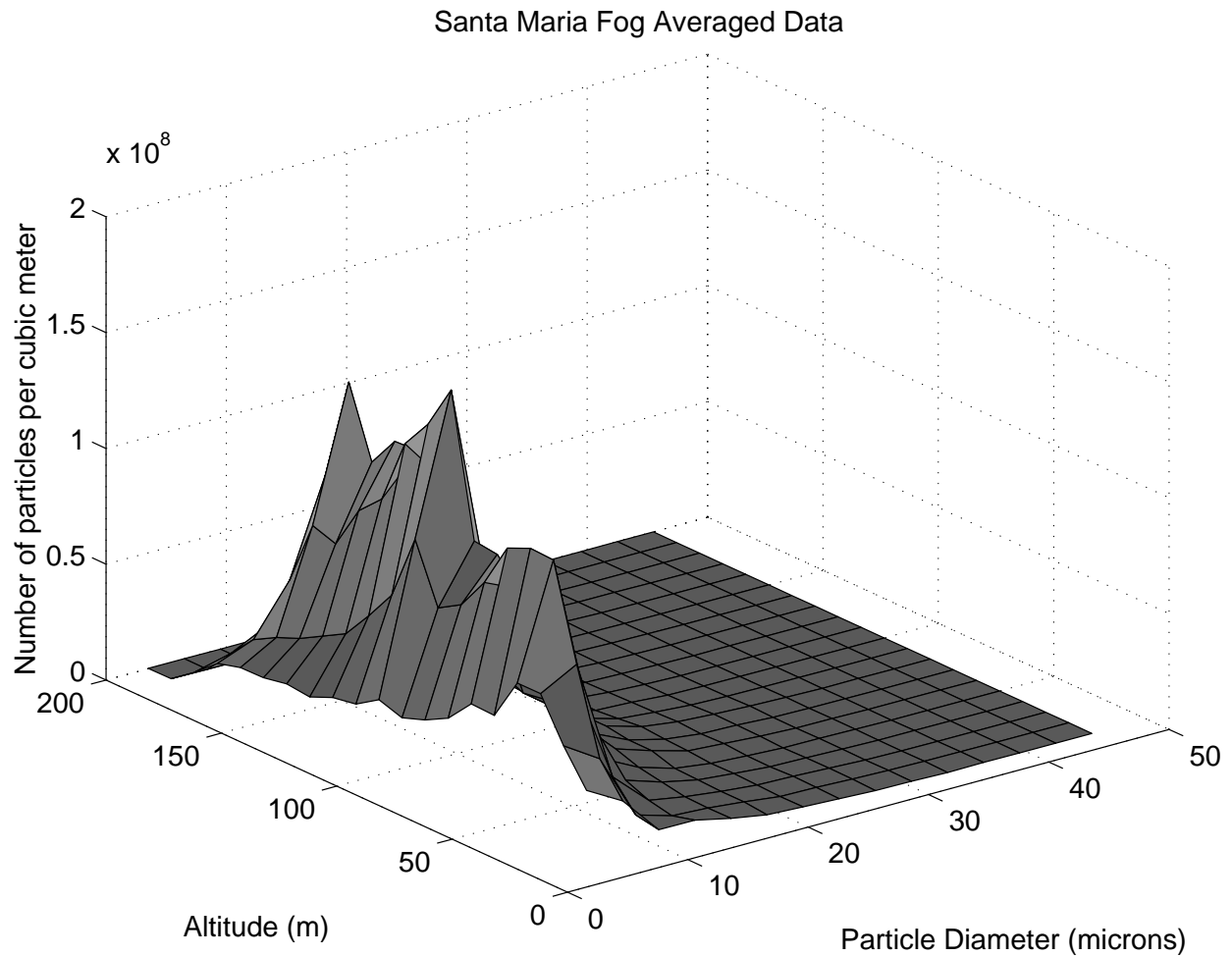
4.2 Data models

Two functions widely used to model atmospheric particle size distributions [9,10,31,12,11] are the gamma and the lognormal distributions. Applied to the available fog data sets, the gamma function is simpler and gives more accurate fits than the lognormal one. However, the lognormal distribution is tested here to fit the data of the VAN and ARC fogs including the 50 - 310 μm diameter range, where the gamma distribution provides a poorer fit.

The inclusion of this range in the fog analysis results in a considerably higher reflectivity factor as defined in (3.9). However, for the earlier mentioned reasons concerning the larger particle data, the implementation of the lognormal model is restricted to the mathematical analysis and the data fit only. The results show that for a more inclusive range (i.e. 2 - 310 µm) of particle sizes the lognormal distribution is more suitable than the gamma one.

4.2.1 Gamma distribution

The gamma distribution can be written as a function of the particle diameter D [m] and the altitude z [m] as follows:

$$n_4(z, D) = n_3(z) N_0 D^\gamma e^{-\beta D} \tag{4.1}$$

where $n_4(z,D)$ is in m^{-4}, $n_3(z)$ is the particle density in m^{-3}, N_0 is a normalizing factor, and β [m^{-1}] and γ are parameters, may dependent on altitude, to be defined by the experimental data.

The data fitting (regression analysis) results in γ values varying between 1 and 7 with a mean value close to 4. Figure 6 shows how γ vary in VAN and ARC through different heights.
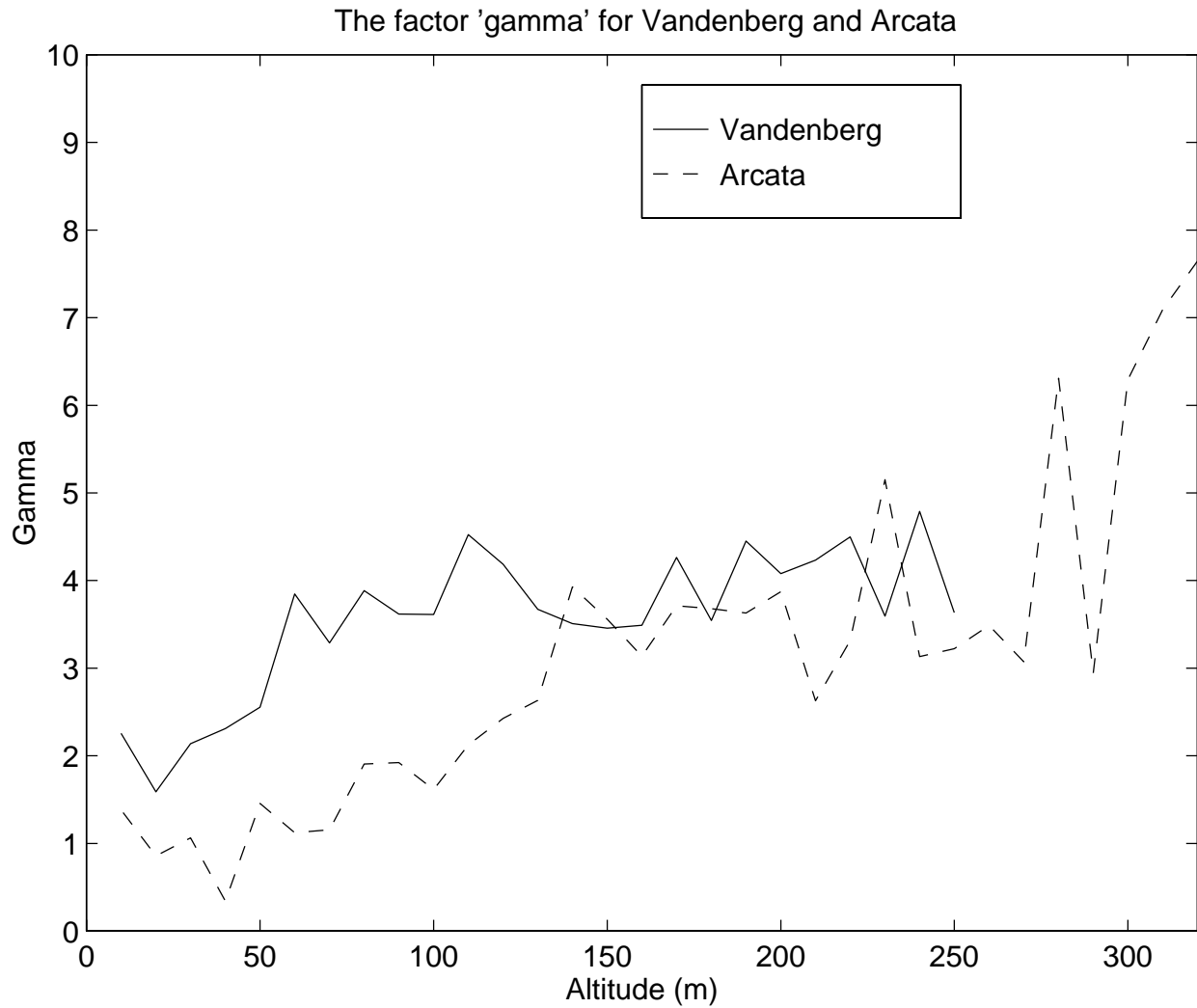
Figure 6. The factor γ for VAN and ARC after the data analysis.

For calculation purposes it would be more efficient to use a constant integer value for γ and do the analysis to find the factor β. The best fit is found for γ = 4 which still gives a very good approximation of the measured size distribution. Figure 7 and Figure 8 show the error in fitting a gamma function to the data with the "general" γ, as resulted after the first analysis, and γ=4, for VAN and ARC respectively. The error *Er* is defined by :

$$Er = \sum_{bin} \left(n_{raw}(D) - n(D) \right)^2 \qquad (4.2)$$

where $n_{raw}(D)$ is the raw data size distribution at a given altitude and $n(D)$ is the modeled size distribution calculated, for each 3 μm bin at the central diameter, using (4.1). The summation is done over the entire number of the bins.
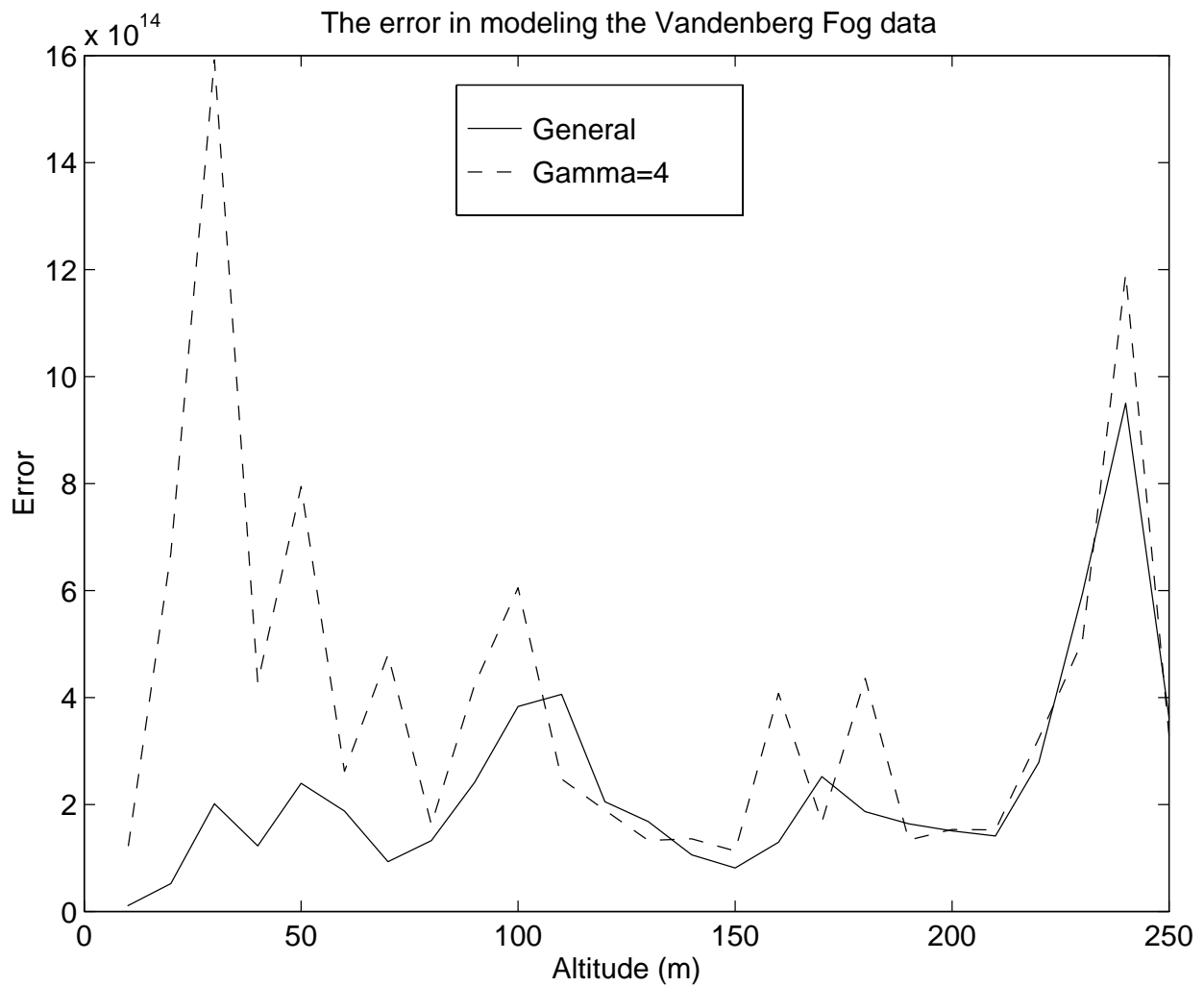
Figure 7. The error in fitting the VAN data using the general γ or using γ = 4.
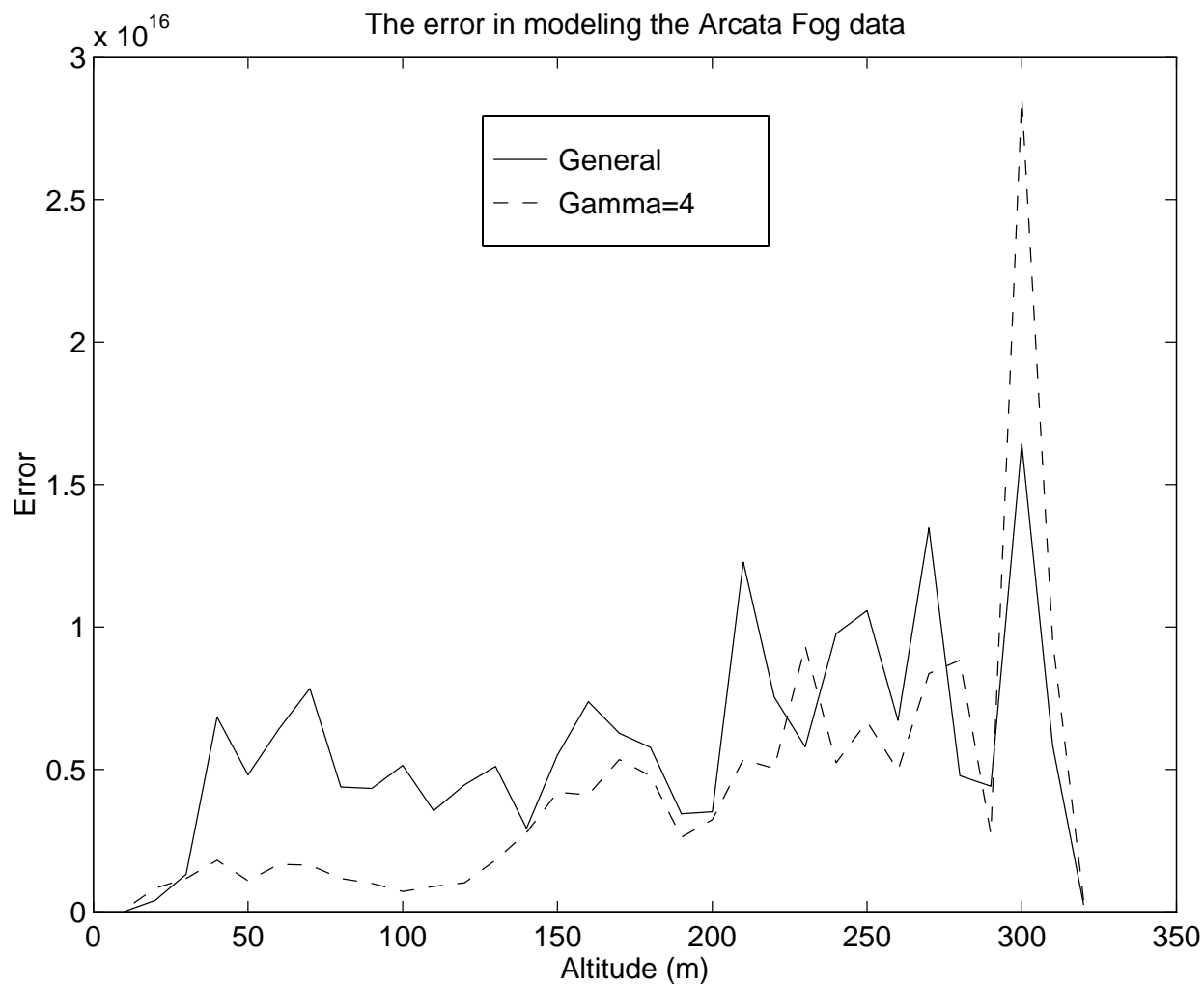
Figure 8. The error in fitting the ARC data using the general γ or using γ = 4.

Figure 9 shows the parameter β as found from the analysis for the five locations for each altitude. As it is shown, β varies slightly with height suggesting the use of a constant value, different though for each fog. Hence, the mean value of β is used in the model of (4.1) simplifying considerably further calculations where the particle size distribution is involved.
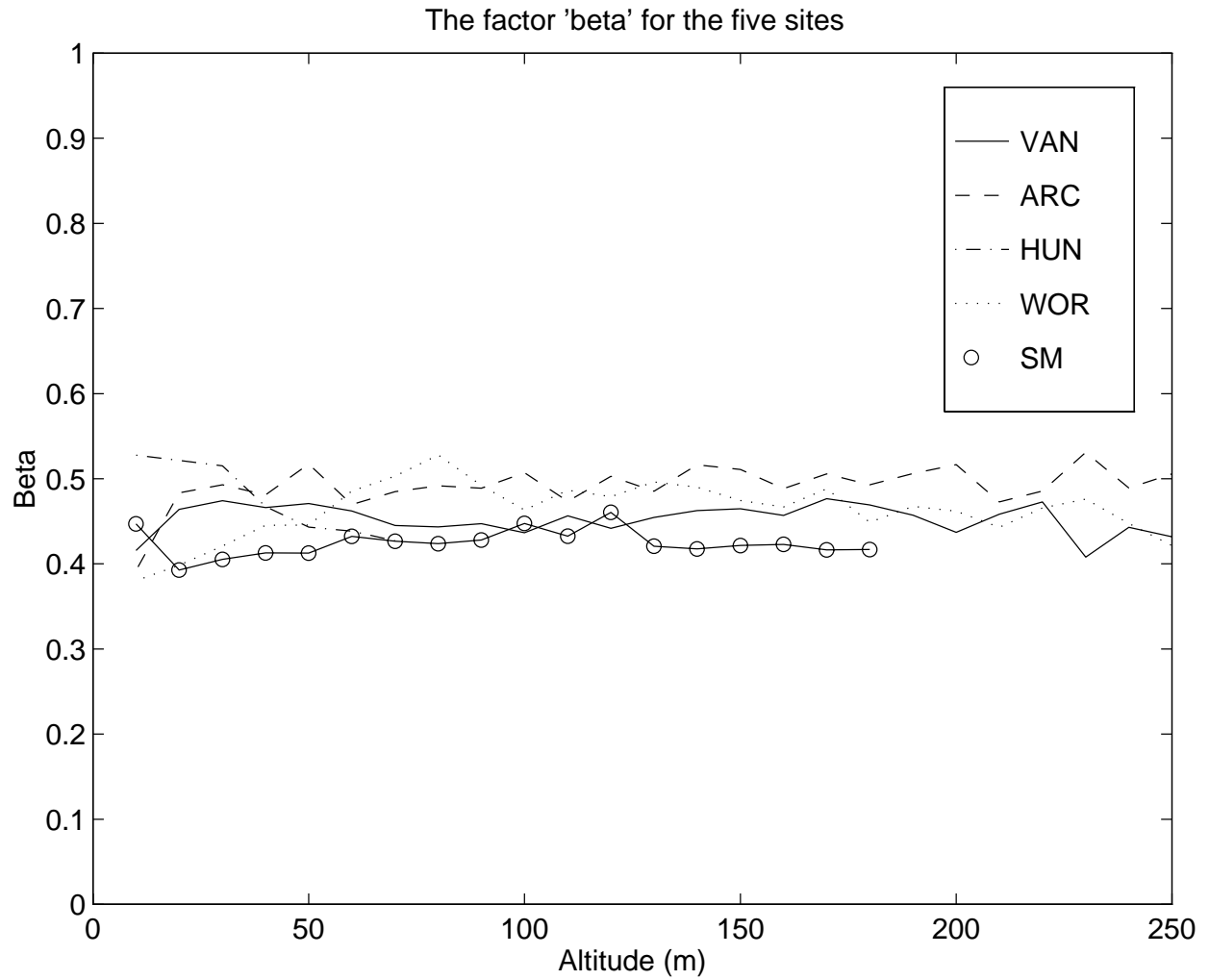
Figure 9. The factor β vs. altitude as found for all the five sites.

In this case, the factor N_0 is determined as follows :

$$n_3(z) = \int\limits_0^\infty dD n_4(z,D) \Rightarrow \int\limits_0^\infty dD N_0 D^4 e^{-\beta D} = 1 \Rightarrow N_0 = \frac{\beta^5}{4!} \qquad (4.3)$$

The size distribution modeling is completed with modeling the particle density $n_3(z)$ by fitting an appropriate function to the average data. Table 1 summarizes the parameter values obtained from the analysis of the data of the five locations (s.d. stands for *standard deviation*).

	$n_3(z)$ in m^{-3}	s.d.	β in μm^{-1}	range of z(m)
VAN	$-12986z^2+3.14\times10^6z+7.14\times10^7$	±97%	0.4527±3.9%	0<z≤250
ARC	$-0.519z^4+316.77z^3-6.88\times10^4z^2+7.11\times10^6z-1.82\times10^7$	±43%	0.4917±5.3%	0<z≤320
WOR	$4.02\times10^4z^{2.5126}e^{-0.0258z}$	±44%	0.4573±7.6%	0<z≤300
HUN	$5.74\times10^6z^{1.3}e^{-0.066z}$	±112%	0.4772±9.1%	0<z≤70
SM	$-3.2788z^4+1.151\times10^3z^3-1.58\times10^5z^2+1.11\times10^7z-2.08\times10^7$	±21.4%	0.4243±3.8%	0<z≤190

Table 1. Summary of the parameters used in the model of (4.1) for each location.

Figure 10 shows a representative fit of the gamma model for VAN at 140 m altitude. Figure 11 shows how the model, averaged over altitude, fits the corresponding average data for VAN.
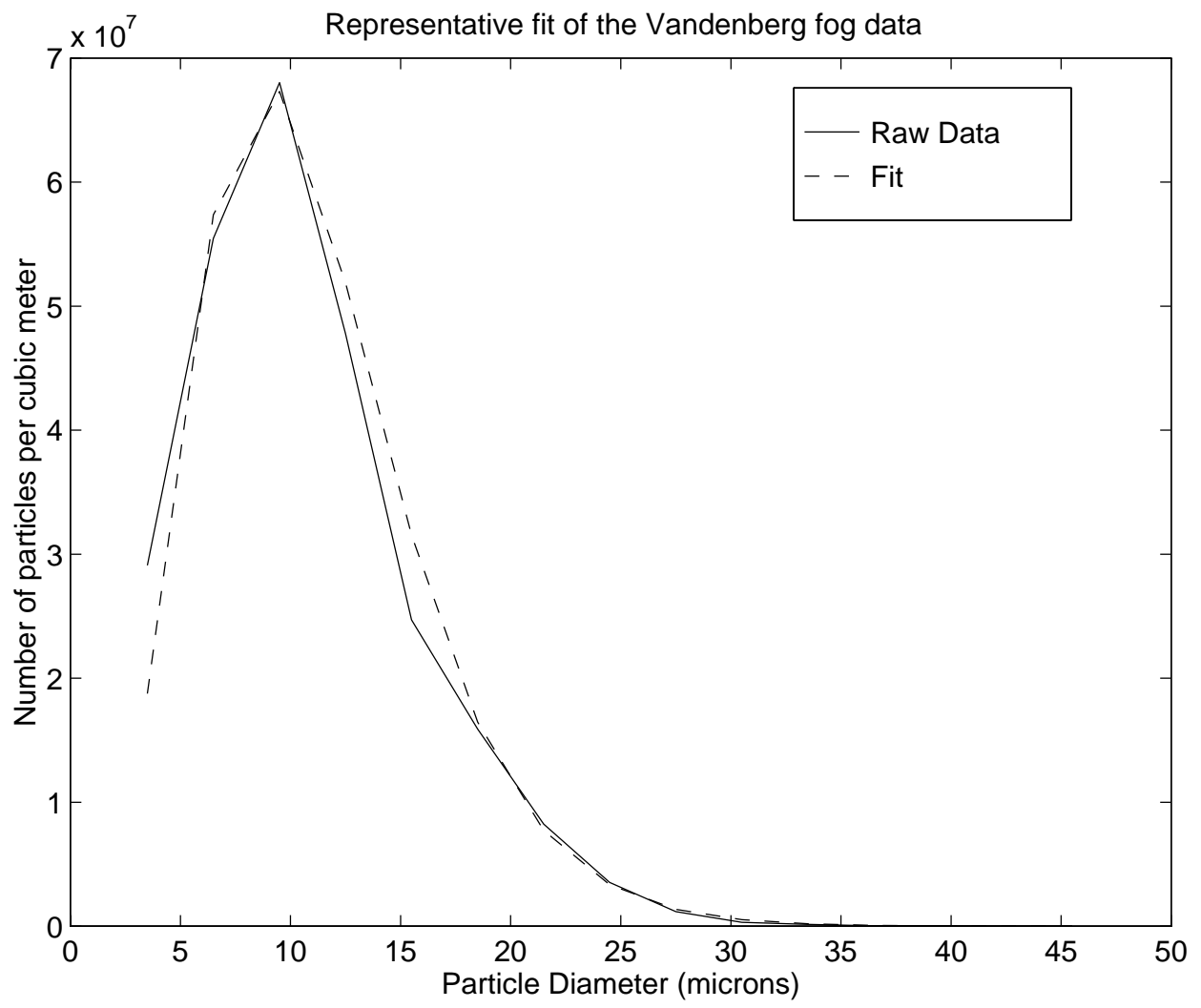
Figure 10. Representative gamma function fit to the VAN data at altitude 140 m.
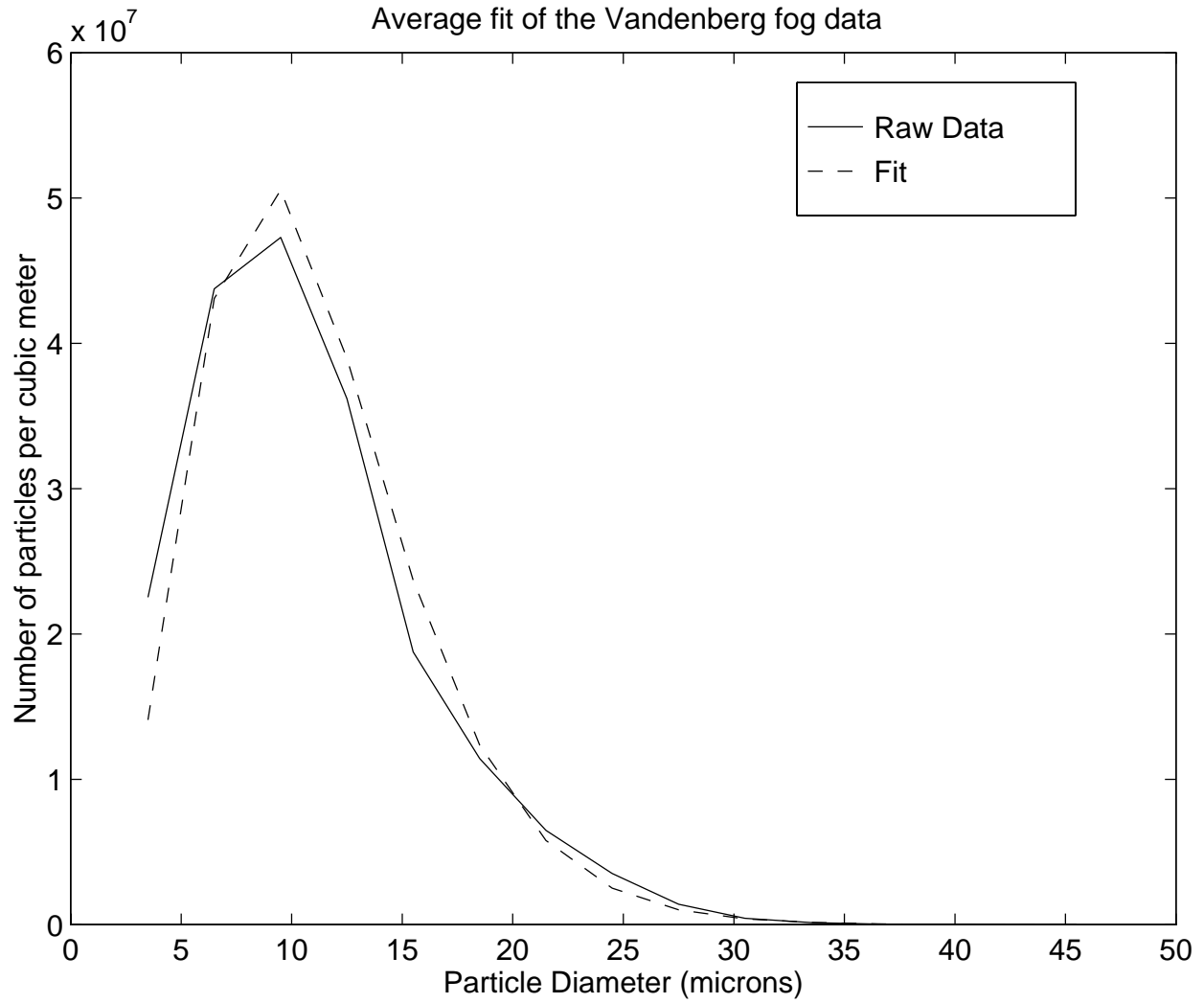
Figure 11. The data averaged over the different altitudes and the average corresponding gamma function fits for the VAN fog layer.

Using the model expressed by (4.1) with γ=4, the liquid water content M and reflectivity factor Z are, respectively, given by:

$$M(z) = \frac{\pi}{6} 7! \rho_w N_0 \beta^{-8} n_3(z) \tag{4.4}$$

and

$$Z(z) = 10! \, N_0 \beta^{-11} n_3(z) \qquad (4.5)$$

Hence, as expressed by (3.12), a linear relationship between Z and M results:

$$Z(z) = \frac{4320}{\pi \, \rho_w} \beta^{-3} M(z) \qquad (4.6)$$

The water content calculated by (4.4) fits the actual water content as it is calculated using the average data very well. Figure 12 shows the fit for the case of the VAN fog.
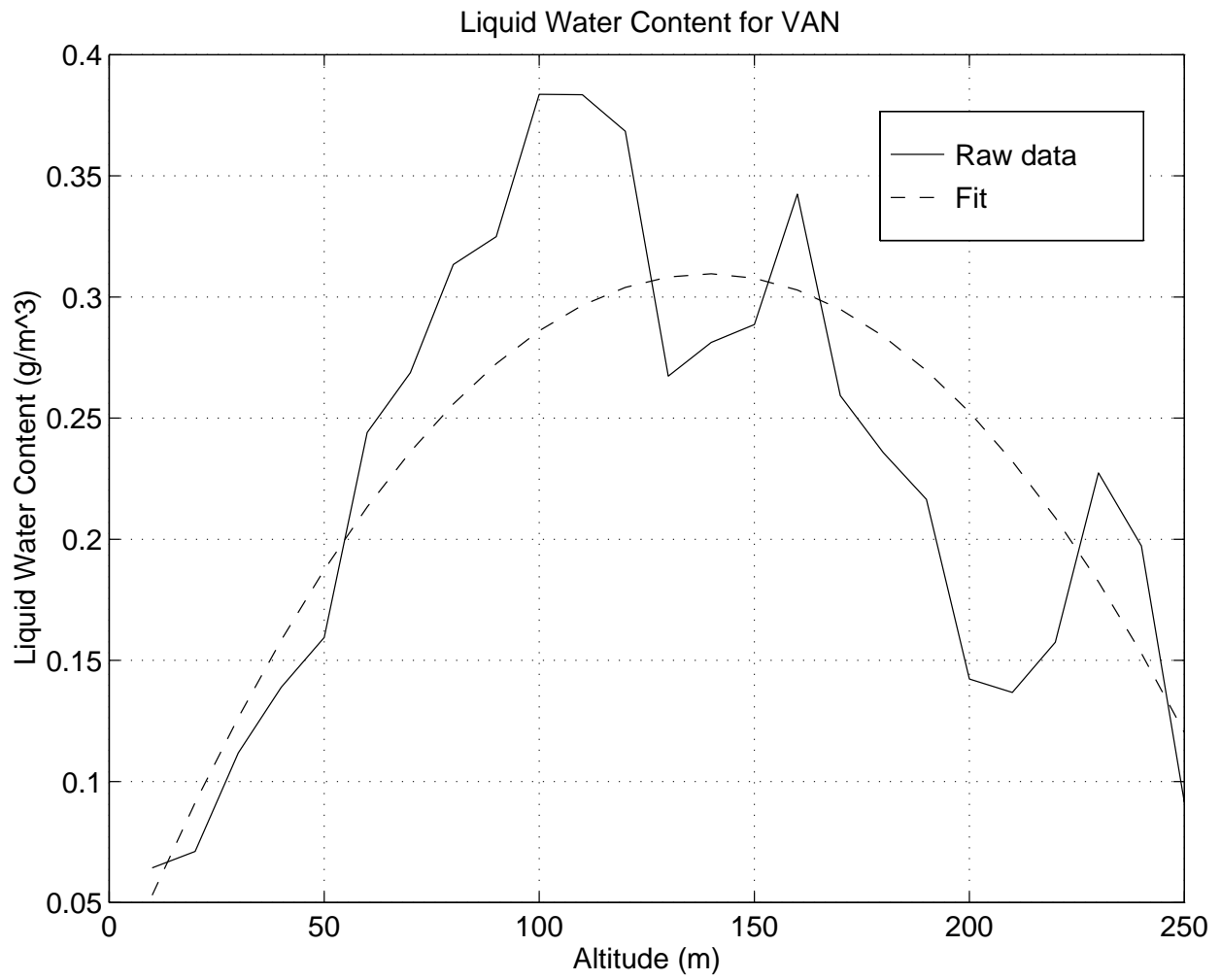
Figure 12. Liquid water content of the VAN fog as it is calculated based on the raw data and using the fit of the equation (4.4).

4.2.2 Lognormal distribution

The lognormal distribution can be written as a function of the particle diameter D [m] :

$$N(D) = \frac{1}{D \ln \sigma_g \sqrt{2\pi}} \exp\left[-\frac{(\ln D - \ln D_g)^2}{2 \ln^2 \sigma_g} \right] \tag{4.7}$$

where D_g, and σ_g are the mean diameter and the standard deviation of the corresponding Gaussian distribution.

By setting $\zeta = \ln D$ and $\zeta_g = \ln D_g$ in (4.7) we have:

$$\int_0^\infty dD N(D) = \int_{-\infty}^\infty d\zeta \frac{1}{\ln \sigma_g \sqrt{2\pi}} \exp\left[-\frac{(\zeta - \zeta_g)^2}{2 \ln^2 \sigma_g} \right] = 1 \tag{4.8}$$

Hence, the altitude dependent particle size distribution $n_4(z,D)$ (m^4) can be written as:

$$n_4(z, D) = n_3(z) N(z, D) \tag{4.9}$$

where $n_3(z)$ is the particle concentration (m^{-3}), and $N(z,D)$ is the same as in (4.7) except for the altitude dependence which is reserved for the case that either D_g or σ_g change by altitude.

The model described in (4.9) was applied for the VAN and ARC fog data. The particle-size distribution data are given in 3 μm bins for particles with diameter 2-47 μm, and 20 μm bins for diameters 10-310 μm. Before the data are used to fit the lognormal distribution function they are averaged over the runs and then used as follows:

- The 2-47 μm data are divided by 3.

- The 50-310 μm data are divided by 20.

- All together, the above, form the set of data for the fit.

Figure 13 shows a representative fit of the function to the VAN data at 190 m altitude. Figure 14 shows how the over the altitude averaged model fits the corresponding average data for VAN.
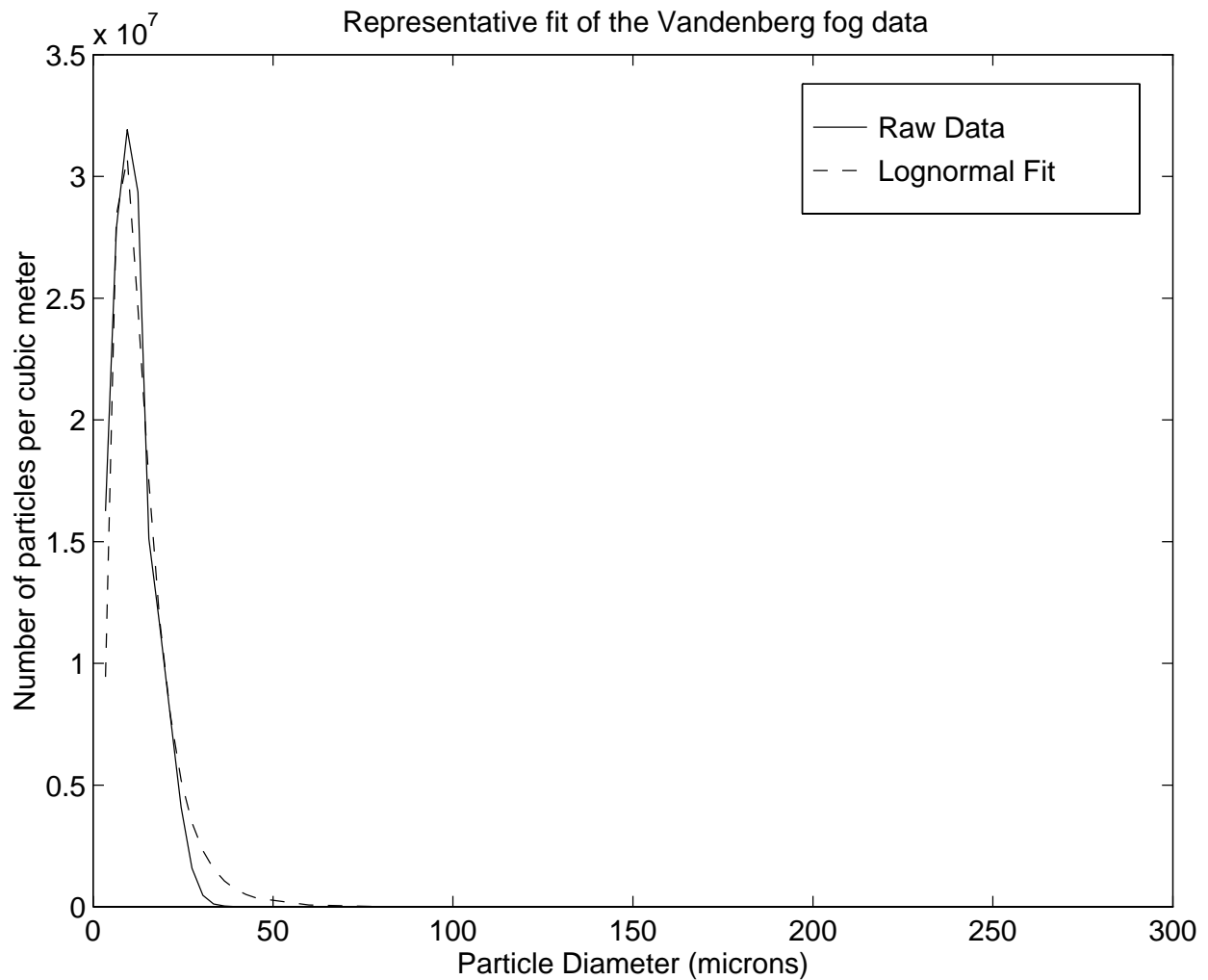
Figure 13. Representative lognormal function fit to the VAN data at altitude 190 m.
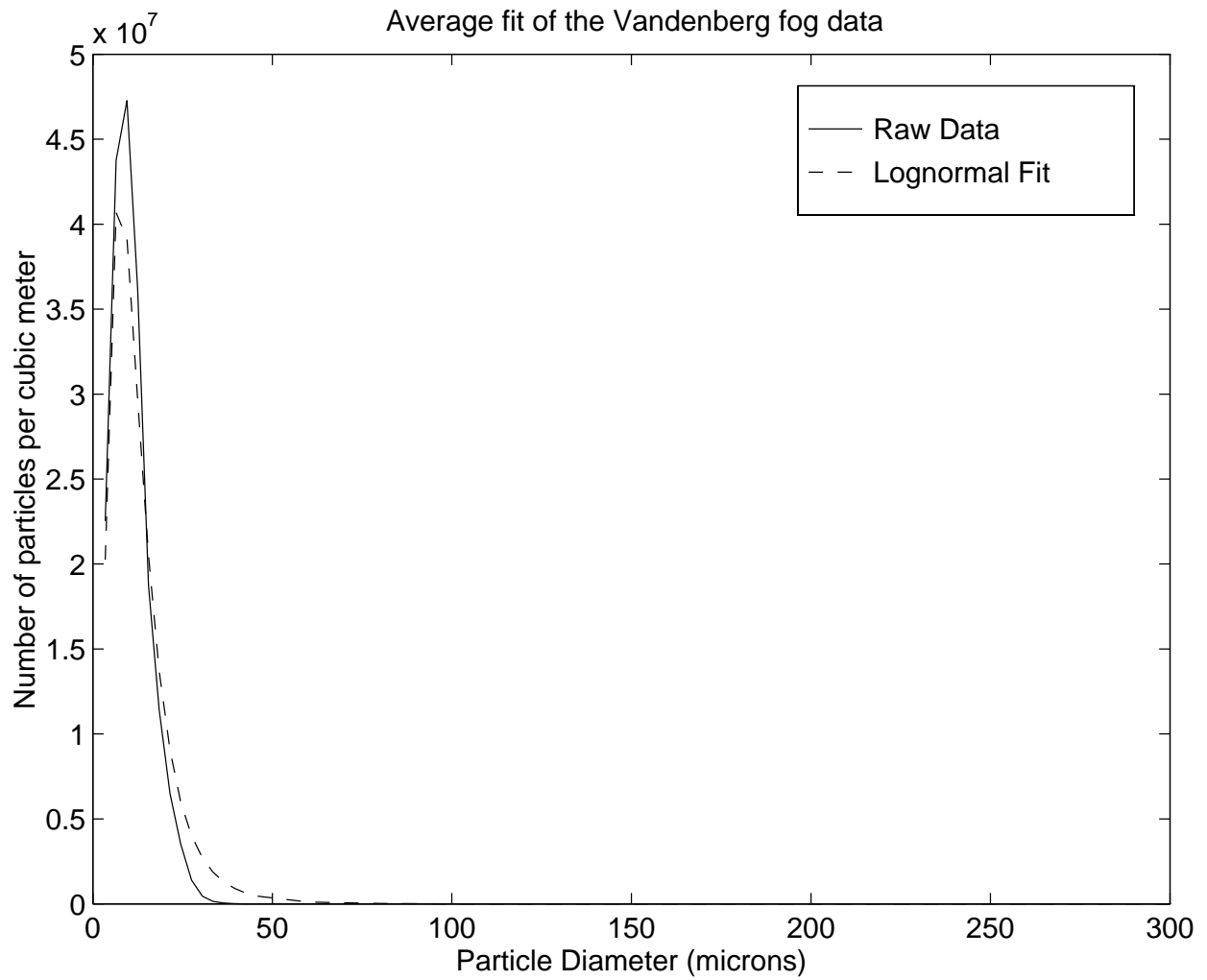
Figure 14. The data averaged over the different altitudes and the average corresponding lognormal function fits for the VAN fog layer.

The parameters D_g and σ_g are found to vary with altitude. This variation is found to be well represented by a linear fit, as summarized in Table 2.

	D_g	σ_g
VAN	0.0131z(m)+9.069	-0.0015z(m)+2.0006
ARC	0.010z(m)+8.317	-9.07×10^{-4}z(m)+1.9247

Table 2. The fit of the altitude dependence of the parameters used in the model of (4.9) for VAN and ARC.

We notice that the particle distribution shifts to larger particles and becomes more spread as we move to higher altitudes. Nevertheless, this is what is expected from the theory [23,2] since temperature, at least for these data, increases with altitude. For this reason, a relationship between the parameters and temperature was tested and the results are summarized in Table 3.

	D_g	σ_g
VAN	$0.4397T(^0C)+3.742$	$-0.0493T(^0C)+2.5988$
ARC	$-0.178T^2(^0C)+4.804T(^0C)-21.41$	$-0.0439T(^0C)+2.2968$

Table 3. The fit of the temperature dependence of the parameters used in the model of (4.9) for VAN and ARC.

It seems that there is no similarity between the two fogs in the way the mean diameter D_g changes with temperature and therefore no useful conclusion can be drawn in this aspect. On the other hand, the spread of the distribution, as it is expressed by σ_g, seems to have a very similar rate of change. However, there is no source found so far to, quantitatively, confirm or contradict the above results.

The particle density $n_3(z)$ in (4.9) is modeled as in the gamma function case and the results of Table 1 apply here as well. Nevertheless, it is important to mention that the model is very sensitive to the two parameters (especially σ_g) and if the mean values, for example, are used instead, then the model is found to be considerably worse. In other words, the altitude dependence of D_g and σ_g must be taken into account.

Using equations (4.7), (4.8), and (4.9) and the definition for the liquid water content (3.7), we have :

$$M(z) = \frac{\pi}{6}\rho_w \int_0^\infty dD D^3 n_4(z,D) = \frac{\pi}{6}\rho_w n_3(z)\int_{-\infty}^\infty d\zeta \frac{e^{3\zeta}}{\ln\sigma_g \sqrt{2\pi}}\exp\left[-\frac{\left(\zeta-\zeta_g\right)^2}{2\ln^2\sigma_g}\right] \tag{4.10}$$

Let $\varphi = \dfrac{\zeta-\zeta_g}{\ln\sigma_g}$. Then $\zeta = \ln\sigma_g\varphi + \zeta_g$ and (4.10) gives:

$$M(z) = \frac{\pi}{6}\rho_w n_3(z)e^{3\zeta_g}\int_{-\infty}^\infty d\varphi \frac{e^{3\ln\sigma_g\varphi}}{\sqrt{2\pi}}\exp\left[\frac{-\varphi^2}{2}\right] =$$

$$= \frac{\pi}{6}\rho_w n_3(z)e^{3\zeta_g}e^{4.5\ln^2\sigma_g}\int_{-\infty}^\infty d\varphi \frac{1}{\sqrt{2\pi}}\exp\left[\frac{-\left(\varphi-3\ln\sigma_g\right)^2}{2}\right] = \tag{4.11}$$

$$= \frac{\pi}{6}\rho_w D_g^3 e^{4.5\ln^2\sigma_g} n_3(z)$$

and similarly, the reflectivity factor (mm^6/m^3) is given by:

$$Z(z) = \int_0^\infty dD D^6 n_4(z, D) = D_g^6 e^{18 \ln^2 \sigma_g} n_3(z) \tag{4.12}$$

where D_g is in (m) in (4.11) and in (mm) in (4.12).

From (4.11) and (4.12) it is inferred that:

$$Z(z) = \frac{6}{\pi \rho_w} D_g^3 e^{13.5 \ln^2 \sigma_g} M(z) \tag{4.13}$$

We see that equation (4.13) suggests, again as (4.6), that a linear relationship between reflectivity and water content should be expected.

5. Results

The theory described earlier along with the results of the experimental data modeling are used to calculate attenuation and reflection in haze and fog. The software developed for these purposes is designed to work for every wavelength using the Mie scattering coefficients [4]. However, the results presented in this section, are derived for some representative wavelengths :

- Visible : 0.5 μm

- Infrared : 2 μm

- Far infrared : 10 μm, which is widely used in applications [33,14]

- 3.2 mm or 95 GHz frequency (W-band)

- 6.8 mm or 44 GHz frequency (Q-band)

- 8.6 mm or 34 GHz frequency (K$_a$-band)

Following are the results for the two types of aerosols presented separately.

5.1 Haze

5.1.1 The size distribution model

Haze is a non-precipitating ensemble of liquid micron−size particles typically found in a shallow surface layer of the atmosphere [22]. It is an ensemble of particles with a size distribution influenced by the size distribution of the original condensation nuclei [24].

The distribution employed for the calculations is a widely - accepted one [35,23,9,18,15,29] and is due to Junge. It is typical for those found in nature where the

concentration is inversely proportional to fourth power of the haze drop diameter. However, the use of this distribution is disputed by some authors [35,11]. As it is stated [11], its simplicity is illusory, since the upper and lower size limits strongly influence the shape of the absorption curve. Alternatively, the modified gamma or the lognormal distribution are suggested by Zuev [35] and Deirmendjian [11], while Whetby [32] suggests a bimodal size distribution, which is the superposition of the other two.

In this case though, where there is lack of other sources - as data - to determine a more precise model, and keeping the above argument in mind, the Junge model is applied as follows:

$$n(z,D) = c(z)\frac{\alpha}{D^4}, \quad \text{for} \quad D_{min} < D < D_{max} \tag{5.1}$$

where D is the haze drop diameter (m), $c(z)$ is the particle density (cm^{-3}), and α is a normalizing factor defined as :

$$c(z) = \int_{D_{min}}^{D_{max}} dD n(z,D) \Rightarrow \alpha = \frac{3}{D_{min}^{-3} - D_{max}^{-3}} \tag{5.2}$$

The diameter bounds are set at D_{min}=0.1 μm and D_{max}=5 μm. The haze layer is considered [22] below z_o = 2 km with peak particle density at z_o and an exponential decay in particle density at $z < z_o$ governed by,

$$c(z) = c(z_o)e^{-(z_o-z)/d} \tag{5.3}$$

where it is specified that d = 440 m (marine haze) and d = 1,100 m (continental haze) and the sensor is assumed to be on board of an airplane that is gliding downwards at an elevation angle θ=3°.

5.1.2 Attenuation

As explained earlier, equation (3.2) is used to calculate the attenuation. The forward-scattering coefficient f(k, D, ε), the square of which is a cross section for forward scatter, is given for spherical particles by the Mie theory. It is a function of the relative dielectric permittivity ε (or refractive index m = √ε) of the particle. The refractive index of haze particles is determined by their composition and by the wavelength of the incident radiation. It can be highly variable [6], particularly because haze particles may have an ice or water layer covering a solid kernel (and water has a refractive index higher than many solid materials). Furthermore, the permittivity of some materials exhibits a strong frequency dependence in the micron wavelength range. We have used a constant representative value $m = 1.33 + 0.35i$ for haze particles observed by the range of frequencies considered in this study. The calculations, however, may require revision because the imaginary part of the refractive index m varies appreciably in this wavelength regime [27].

For the attenuation between the ground and an altitude $z < z_o$ of the airplane we have :

$$S_i(z) = \frac{2\pi}{k \sin\theta} \int_0^z d\zeta \int dD n(\zeta, D) f(k, D, \varepsilon) \tag{5.4}$$

For higher altitudes we measure $S(z_o)$. Insertion of Eq. (5.3) into Eq. (5.4) yields,

$$S_i(z) = d\left(1 - e^{-z/d}\right) e^{-(z_o - z)/d} s_i(z_0),$$

$$\tag{5.5}$$

$$s_i(z_0) = \frac{2\pi}{k \sin\theta} \int dD n(z_o, D) f(k, D, \varepsilon).$$

Graphs of one-way attenuation, $-10\log_{10} S_i(z)$, are plotted as a function of airplane height z for representative wavelength groups in each of the spectral regimes of interest. This for the marine

environment (d = 440 m) can be found in Figure 15, and those for the land environment (d = 1,100 m) in Figure 16. A typical value used for particle density, representing a fairly dense haze in both cases, is $c(z_0)$=3,000 particles/cc. Attenuation is larger at the shorter wavelengths, and it is clearly more serious over land than over sea. However, the attenuation for most wavelengths and heights is negligible except for visible wavelengths in both hazes and the infrared for the continental one.
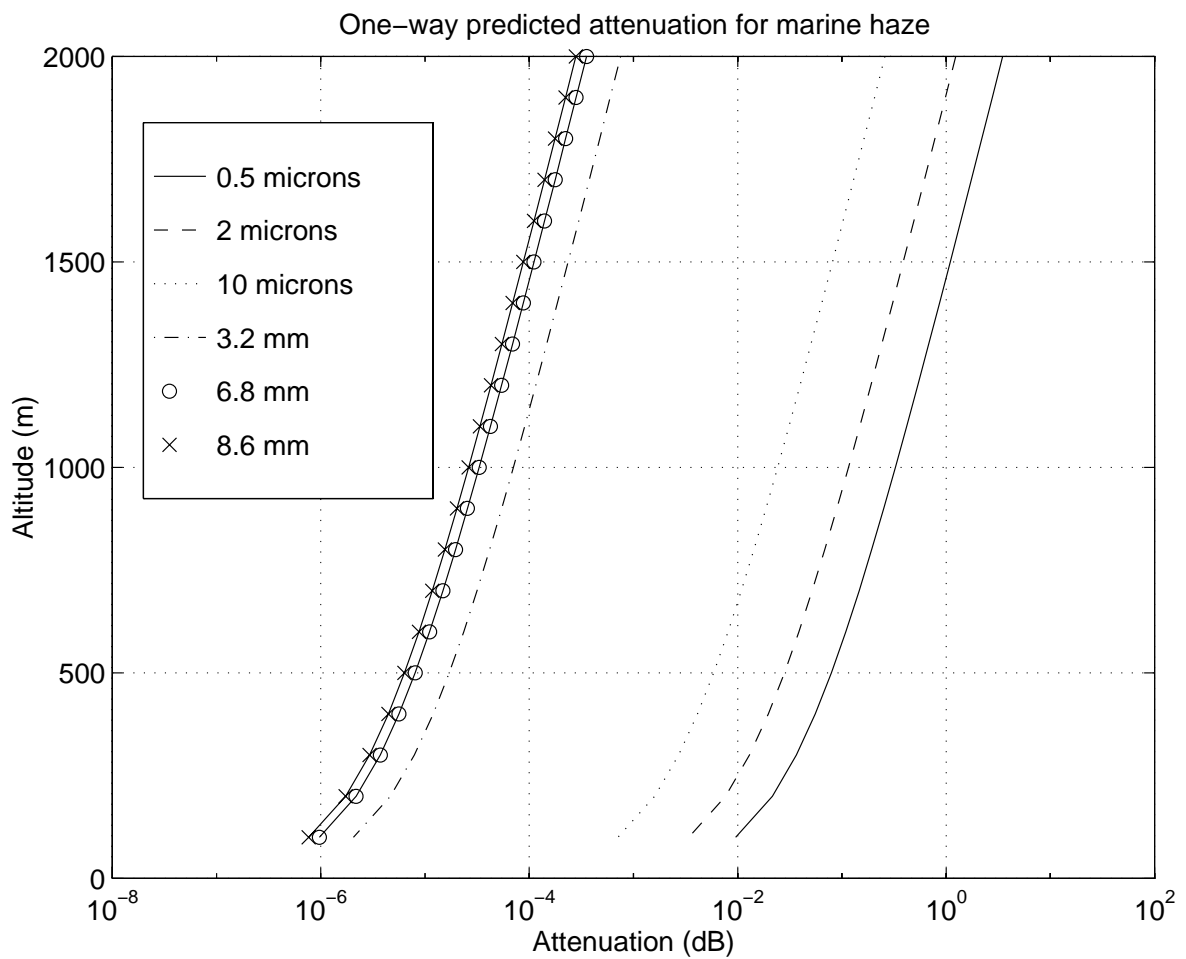
Figure 15. One-way predicted attenuation for marine haze with 3,000 particles / cm^3.

One−way predicted attenuation for continental haze
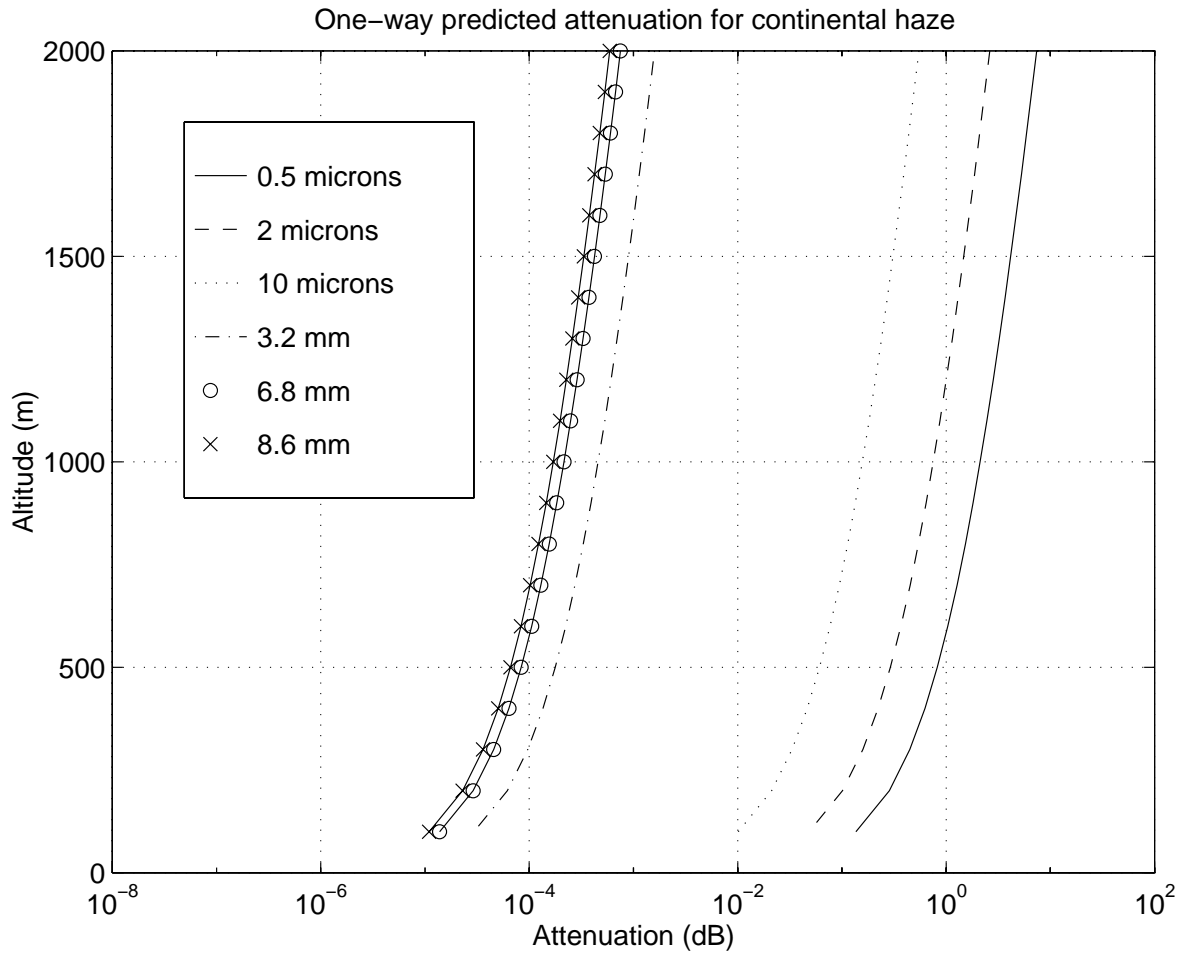
Figure 16. One-way predicted attenuation for continental haze with 3,000 particles / cm^3.

5.1.3 Reflection

We consider the situation in which an airplane sensor gliding in at 3° elevation at altitude $z > z_o$ processes its reflected signal to come from a range-cell region at altitude $z_f < z_o$. The cross section Q for reflection from a unit volume is given by :

$$Q(z_f) = e^{-4S_i(z_f)} q(z_f)$$

$$(5.6)$$

$$S_i(z_f) = \int_{z_f}^{z_o} d\zeta \, s_i(\zeta) = \frac{d}{\sin\theta} \left(e^{-z_0/d} - e^{-z_f/d}\right) e^{z_0/d} s_i(z_0)$$

where q is given in (3.6) and s_i in (5.5). Note that Q is specified in m^2/m^3 .

Figure 17 (marine environment) and Figure 18 (land environment) show graphs of $10\log_{10}$ (Q in m^2/m^3) vs. range-cell altitude z_f for the representative visible to infrared wavelengths, and particle density $c(z_0)$=3,000 particles/cc. We see that the level of the reflected power is higher at shorter wavelengths. Reflection from marine haze seems smaller than the one from continental. In both cases, the difference of the reflection between the different wavelengths is noticeably high.
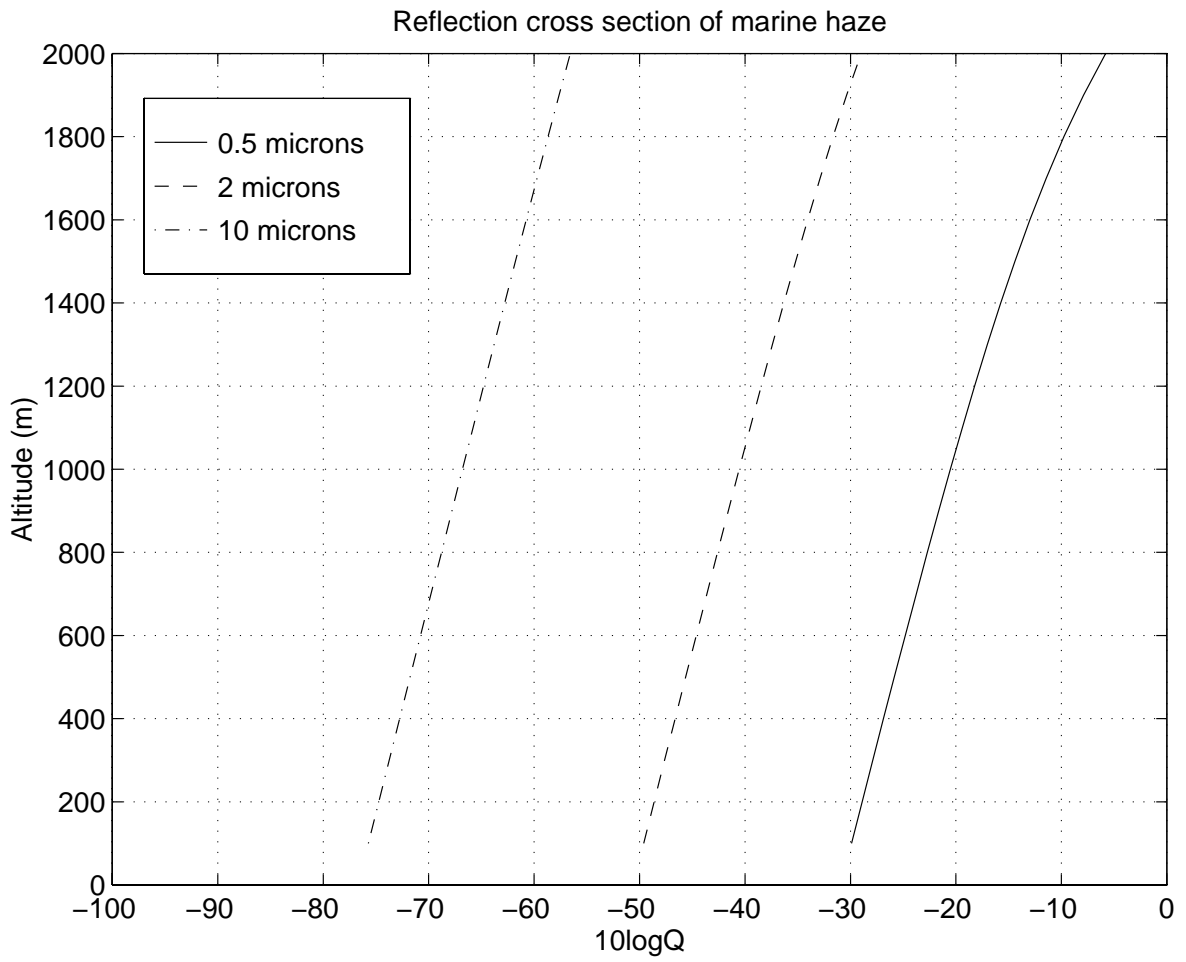
Figure 17. Reflection cross section of Visible and IR along a glideslope in a 3,000 particle cm^{-3} Marine haze layer.
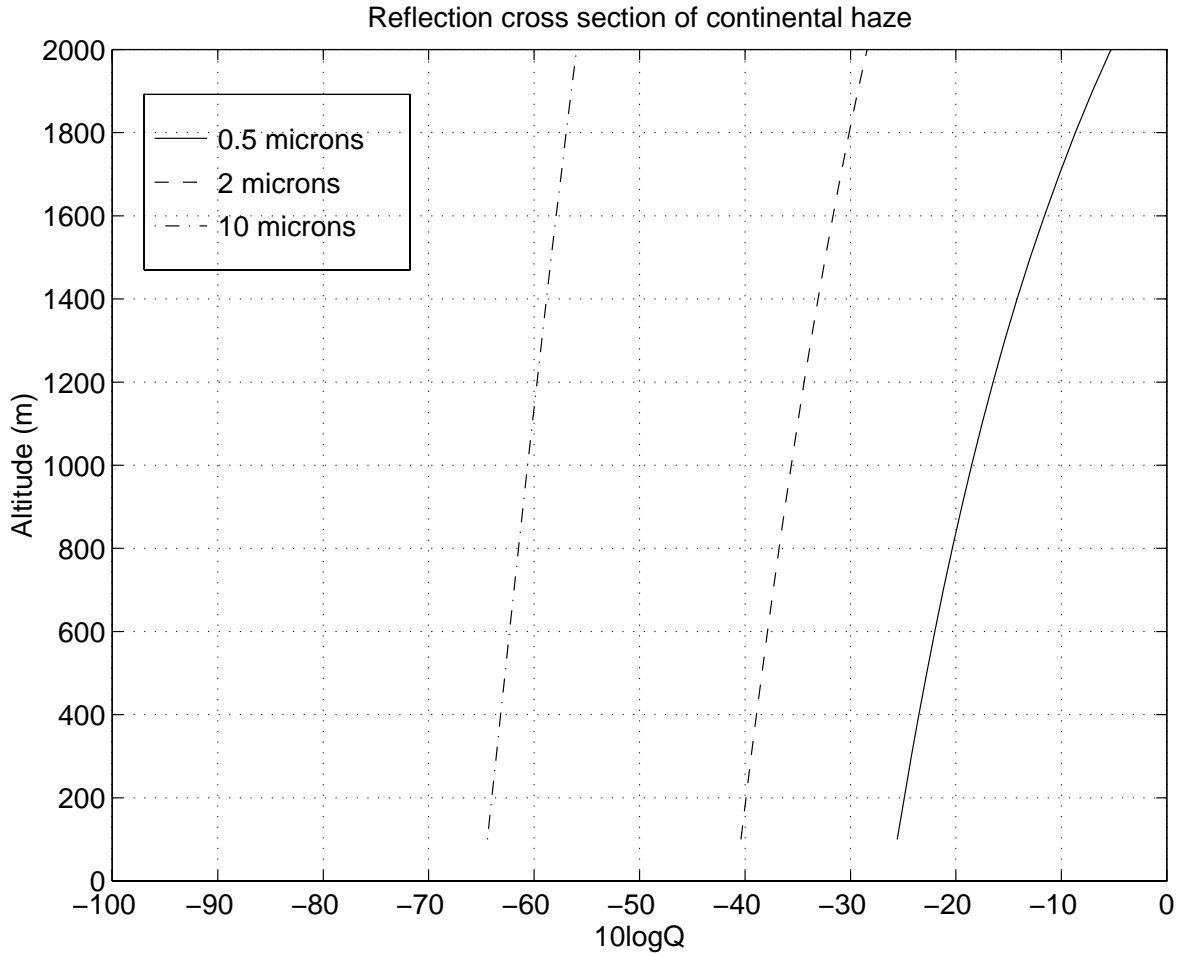
Figure 18. Reflection cross section of Visible and IR along a glideslope in a 3,000 particle cm^{-3} Continental haze layer.

It should be noted that the calculations in (5.5), involving (3.6), are based upon the Rayleigh backscatter cross section for dielectric spherical particles, (3.9). Use of the Rayleigh expressions requires $D \ll \lambda$. The particle diameters range from 0.1 to 5 µm, and the mean diameter is close to 0.15 µm. Hence the calculations are probably fairly accurate for the 2-5 µm and the 10-12 µm spectra, but they may be only marginally correct for the 0.4-0.7 µm spectrum (possibly with a few dB error). The reflection cross section for these high-frequency sensors probably should be recalculated with the proper Mie backscatter cross sections.

5.1.4 Visibility

In order to apply Eq. (3.14) to find the visibility we first have to calculate the extinction coefficient *b*. For the horizontal visibility we have [21] :

$$b = \frac{4\pi}{k} \int dD n(z,D) f(k,D,n) = \frac{4\pi}{k} \alpha\, c(z) \int dD D^{-4} f(k,D,n) \qquad (5.7)$$

where *f(k,D,n)* is the imaginary part of the (forward-scattering) Mie coefficient at given wavenumber *k* and refractive index *n* for a particle with diameter *D*. The particle distribution *n(z,D)* is described in (4,1). The Mie-coefficient is calculated for wavelength $\lambda = 0.55$ μm, which is chosen as a representative wavelength in the visible range. We assume that the haze layer is uniform at same heights.

For the marine haze, where density ranges from 10 to 3,000 cc^{-1}, the minimum visibility ranges, approximately, from 12,900 km to 43 km respectively. For the continental haze, where density ranges from 300 to 10,000 cc^{-1}, the minimum visibility is found to range from 430 km to 13 km respectively. Nevertheless, the long range visibility numbers found are not realistic since molecular absorption in clear air limits visibility to about 340 km [35,13].

From the numbers above it becomes obvious that the ground is always visible from any height; the minimum visibility is 13 km and the haze layer is bounded at 2 km. Therefore no vertical visibility calculations are necessary.

5.2 Fog

5.2.1 Attenuation

Similarly, as in the case of haze, the attenuation is calculated using (5.4). The particle distribution is modeled with a gamma distribution with parameters shown in Table 1. The calculations of the refractive index of water are based on Ray [27].

Figure 19 shows the one-way mean predicted attenuation for VAN, $-10\log_{10}S_i$ (z), as a function of airplane height z landing in a 3^0 glideslope, for the representative wavelengths in each of the spectral regimes of interest. It is clear that for the visible - IR wavelengths the attenuation level is extremely high; above 50 m in altitude it is predicted to exceed 100 dB ! The millimeter wavelengths undergo very small attenuation except the 95 GHz case where at the higher altitudes the attenuation is low yet critical.

Using (5.7) and gamma distribution model for the attenuation coefficient, the ratio $b(z)/M(z)$, M the liquid water content, is independent of altitude. This is certainly the case for the Rayleigh regime as expressed in (3.8). It is shown as a continuous function of wavelength in the millimeter–to–visible regime in Figure 20, and the average and standard deviation, of all five sites, are depicted.

Especially, for the wavelength 10.6 μm, which is of particular interest [26,3,33,14], the b/M ratio ranges from about 619 to about 661 $(dBkm^{-1})/(gm^{-3})$ for the five sites with average 638 $(dBkm^{-1})/(gm^{-3})$. This is in very close agreement with experimental results found in the literature (610 dB/km [26] and 630 dB/km [14]).
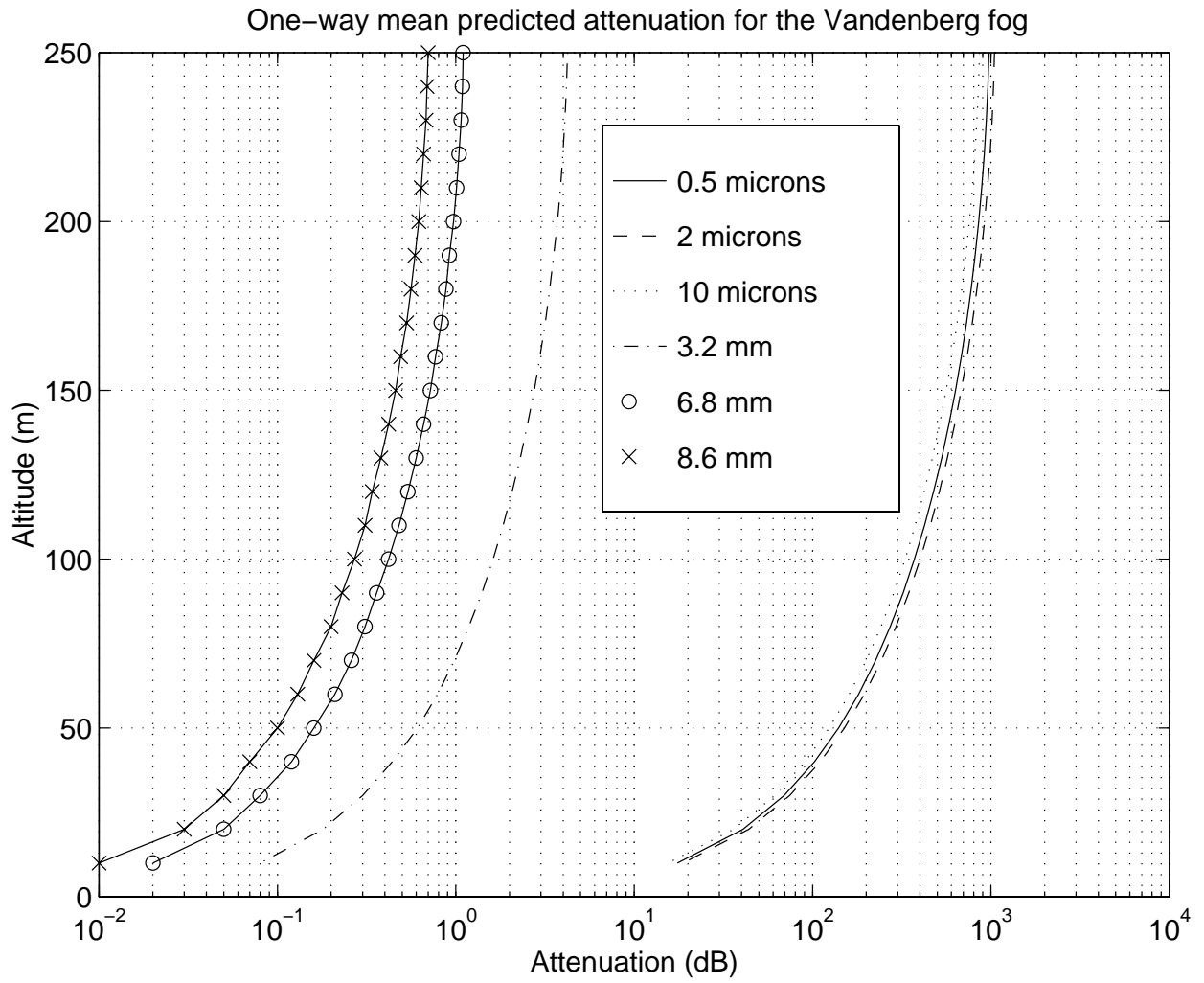
Figure 19. One-way mean predicted attenuation for VAN and various wavelengths.
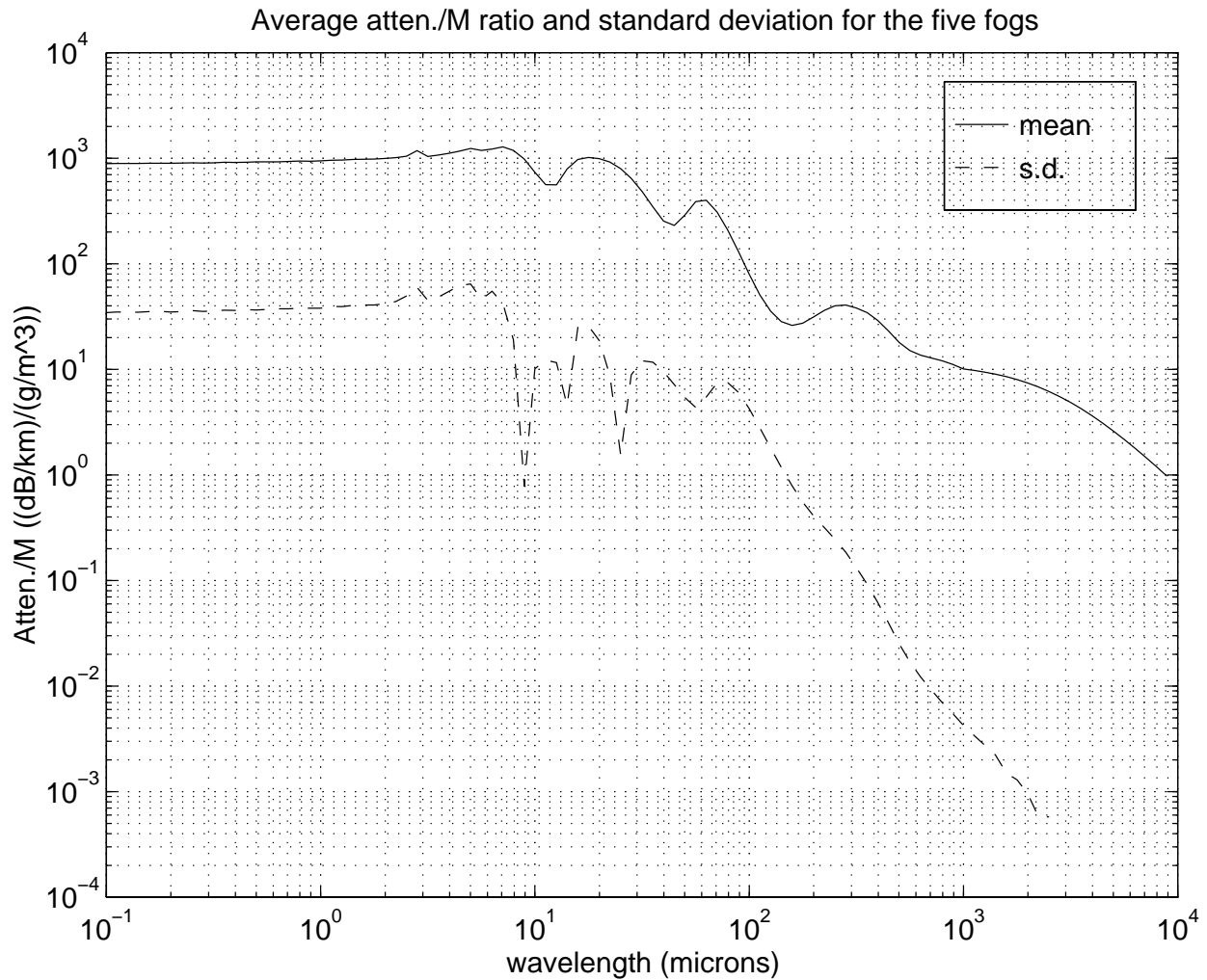
Figure 20. Average attenuation / water content ratio and the standard deviation for the five locations.

5.2.2 Reflectivity Factor and Liquid Water Content

The fog data that are available give us the chance to test the relationship between the Reflectivity Factor Z and the Liquid Water Content M. What is expected from the distribution model analysis and expressed in equations (3.12), (4.6) and (4.13), is a linear relationship

between Z and M. The widely accepted empirical form (3.13), though, suggests a quadratic relationship.

Figure 21 and Figure 22 show the liquid water content M (in gm^{-3}) and the reflectivity factor Z (10logZ in dBZ), respectively, calculated by using the average fog data for the five locations. A test of the Z/M ratio is shown in Figure 23 (10log(Z/M)). We see that, especially for VAN and ARC, the ratio appears to be independent of the altitude as it is expected from the distribution model analysis. In Figure 24, a graph of 10logZ vs. M, based on the VAN and ARC data, is shown for M>0.09 gm^{-3} to test the empirical quadratic relationship (3.13). We see that for the low M values this relationship is good for ARC but it underestimates reflectivity for VAN at about 5 dBZ. For the higher M values it is good for VAN but it overestimates reflectivity for ARC at about 5 dBZ.
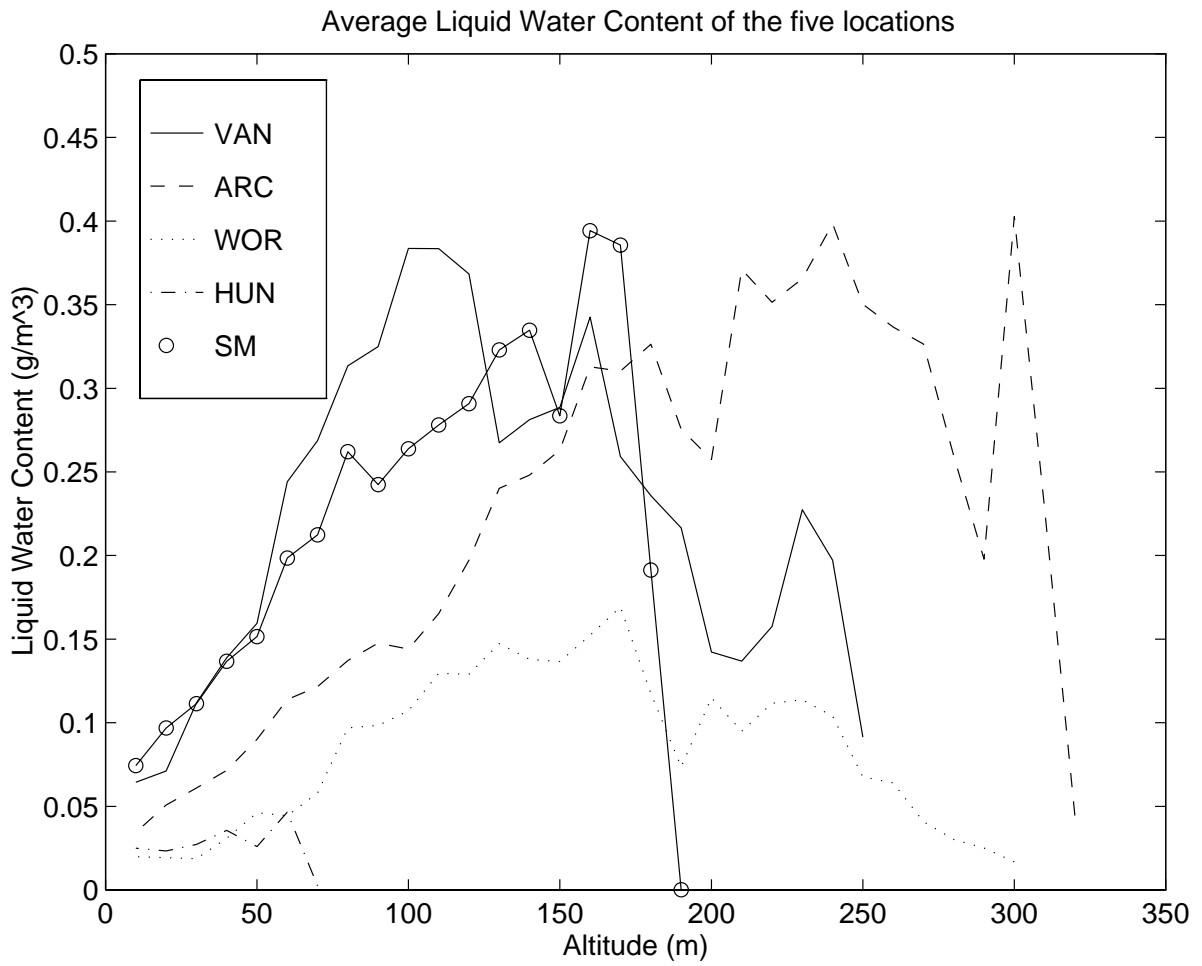
Figure 21. Liquid water content calculated of the five locations using the average data.

Radar Reflectivity Factor of the five locations
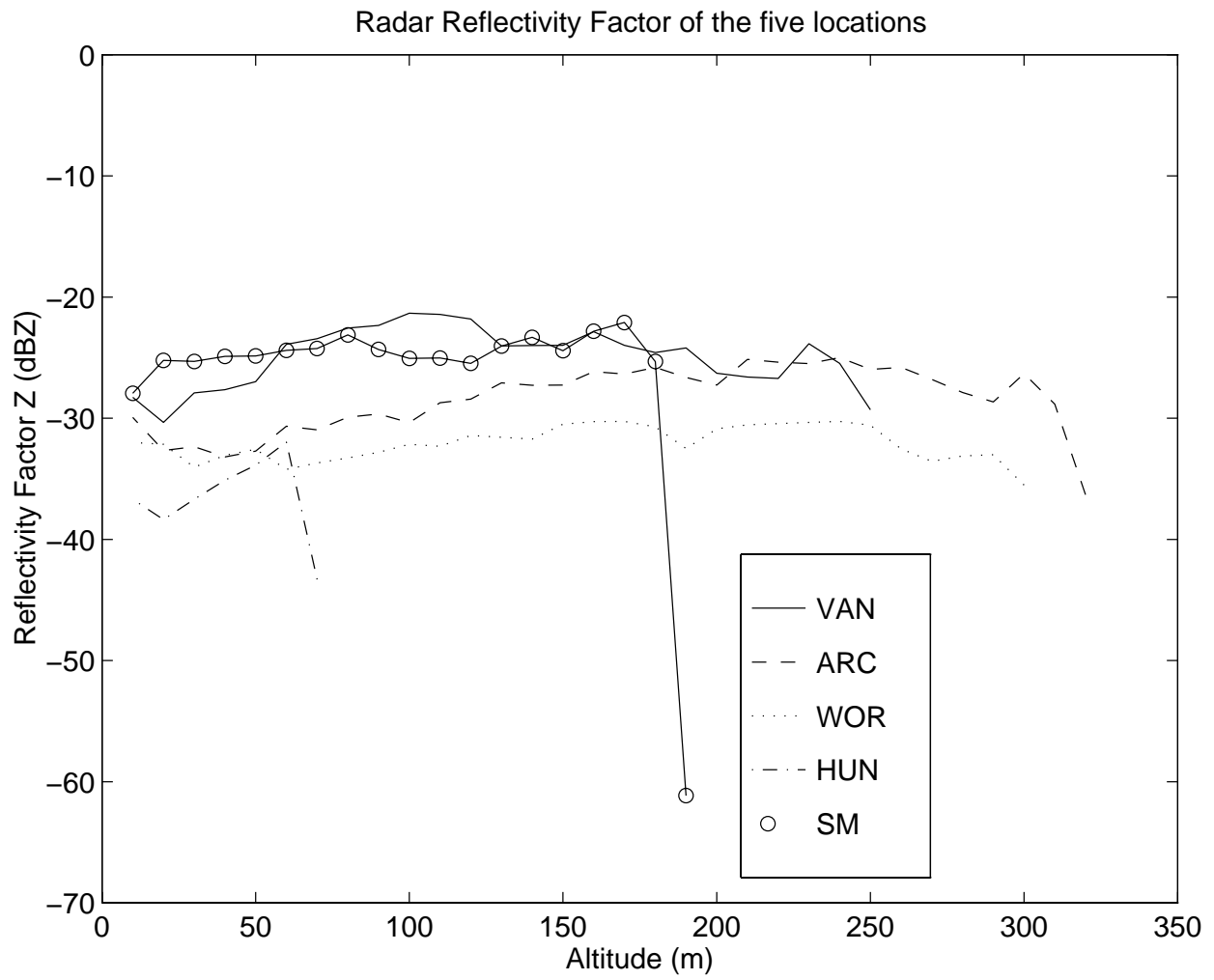
Figure 22. Reflectivity factor calculated using the average data of the five locations.
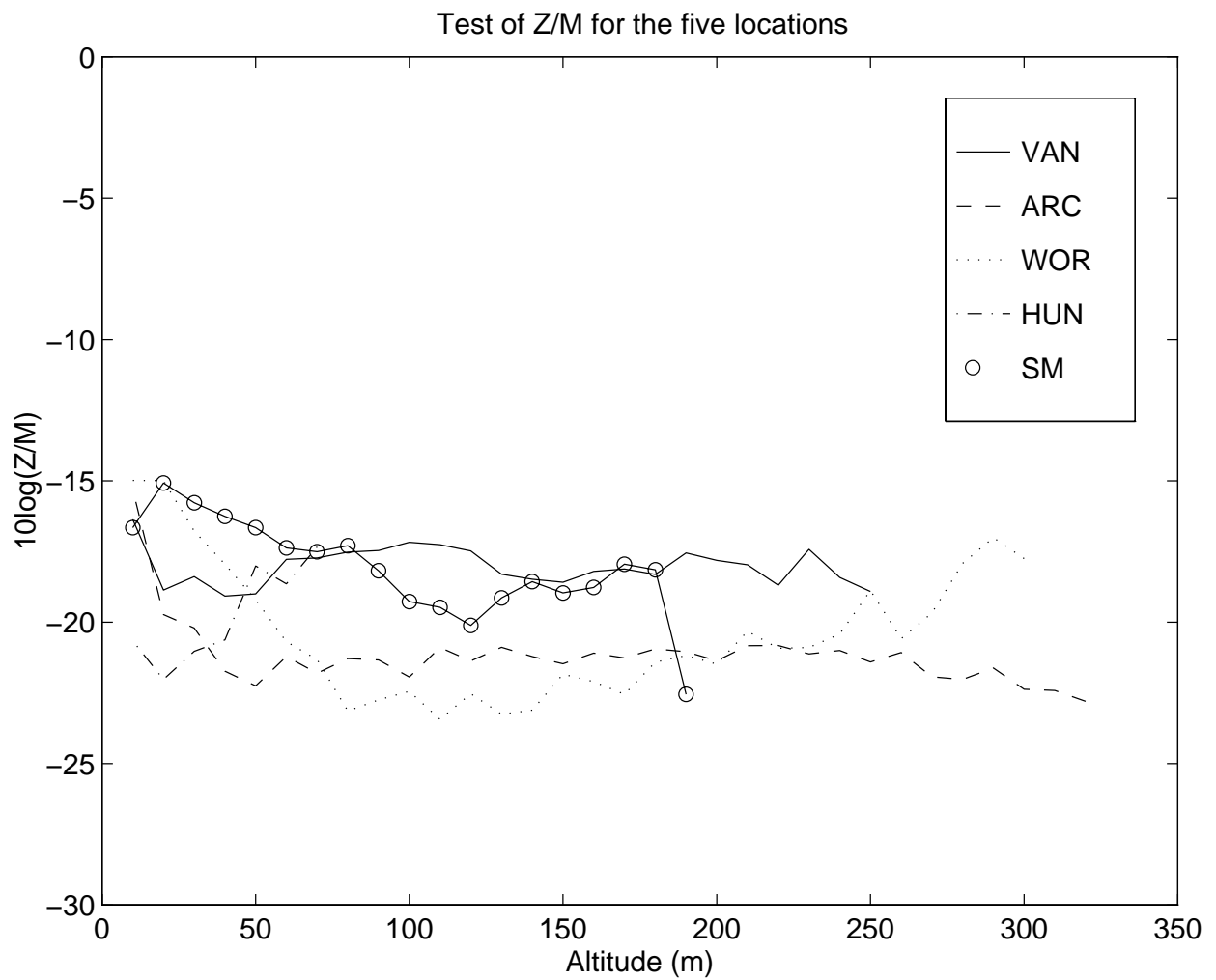
Figure 23. Test of the Z/M ratio for the five locations.
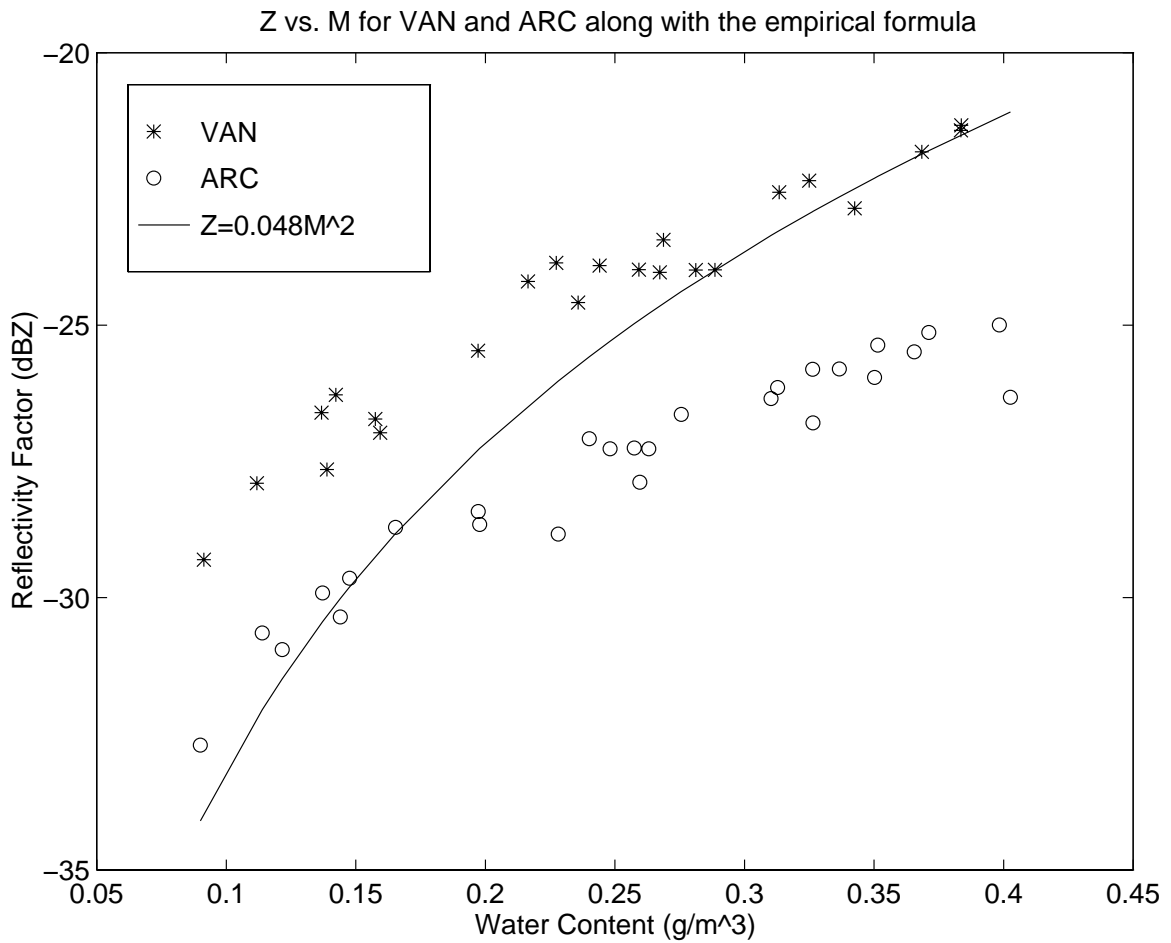
Figure 24. 10logZ vs. M for VAN and ARC together with the empirical relationship Z=0.048M^2.

This discrepancy in predicting Z from M by using (3.13) leads us to seek for other power law relationships that better model the measured Z – M relationship.

Figure 25 shows graph of lnZ vs. lnM, for VAN and ARC, and the resulted power law fits. The regression analysis yields a very good approximation :

VAN: $Z = (0.0211 \pm 5.9\%) M^{1.201}$ (5.8)

ARC: $Z = (0.0081 \pm 2.9\%) M^{1.08}$ (5.9)

Only these two sites have enough data runs so that the average values would overcome the low-threshold limitations sufficiently.
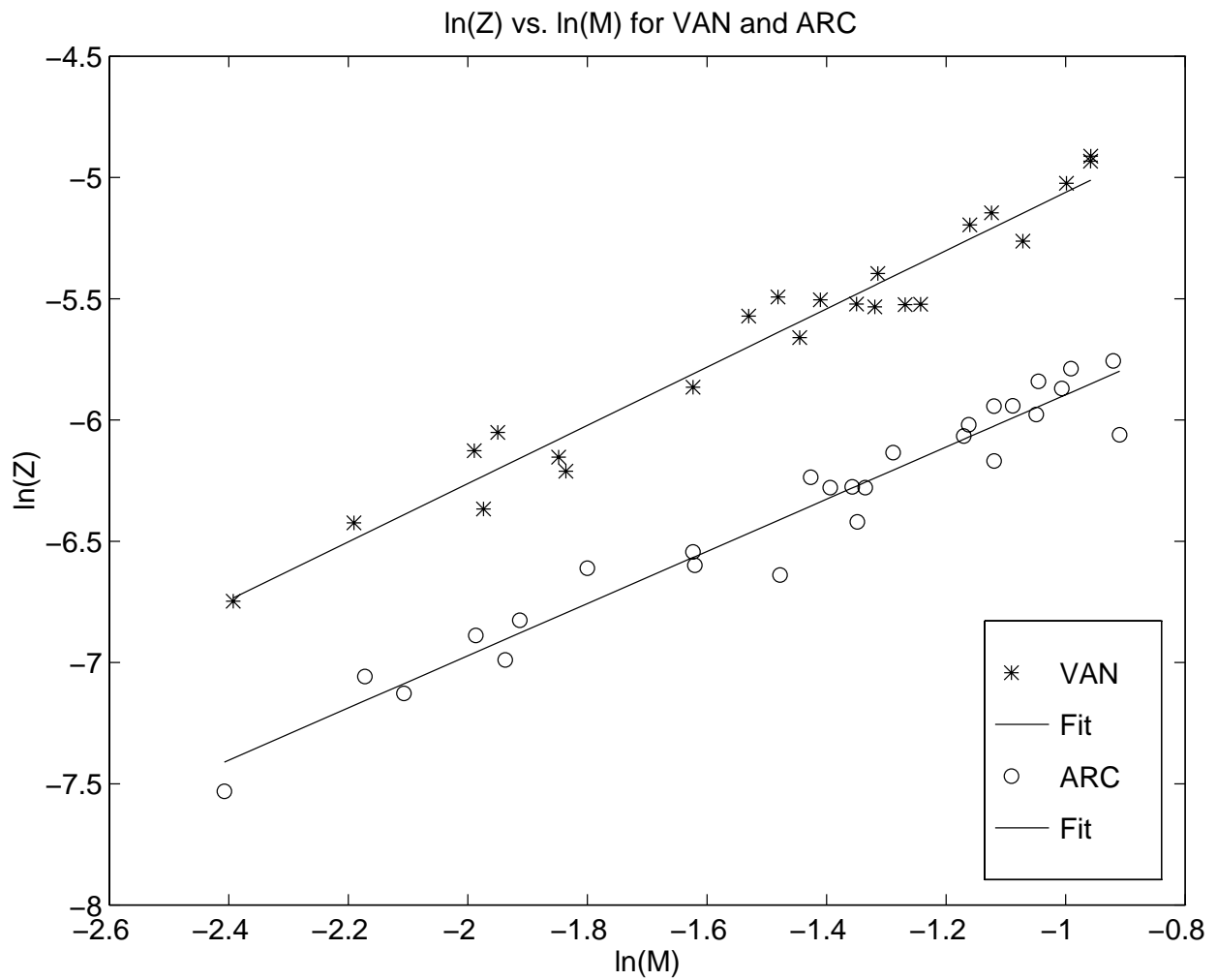
Figure 25. Ln(Z) vs. ln(M) for VAN and ARC to test for a power law relationship.

It should be pointed out, though, that the power-law relationships developed here have been calculated from measured distribution data, whereas the empirical quadratic law (3.13) is based on radar measurements of Z. The radar measurements take into account drops that are possibly not registered in these data or too few and registered as zero. This would result in a measured reflectivity factor higher than the one predicted based on the size distribution measurements. For these reasons it is not straight-forward to predict a $Z - M$ relationship under the conditions of these measurements.

5.2.3 Visibility

As for haze, equation (5.7) is used to calculate the extinction coefficient b for the horizontal visibility :

$$b = \frac{4\pi}{k} \int dD n(z,D) f(k,D,n) = \frac{4\pi}{k} N_0 n_3(z) \int dD D^4 e^{-\beta D} f(k,D,n) \tag{5.10}$$

where $f(k,D,n)$ is the imaginary part of the (forward-scattering) Mie coefficient at given wavenumber k and refractive index n (given by Ray [27]) for a particle with diameter D. The particle distribution $n(z,D)$ is well described in another report [21]. The Mie-coefficient is calculated for wavelength $\lambda = 0.55$ µm, which is chosen as a representative wavelength of the visible range.

The visibility is also calculated using the empirical formula of (3.15) based on the liquid water content both measured and modeled. The results for VAN are shown in Figure 26. The solid line shows the visibility calculated by using (3.15) on the measured data and the dashed line shows the visibility calculated by using (3.14) and (5.10). The empirical law relationship seems to underestimate slightly the visibility but it is still in good agreement with the analytically predicted one.

Figure 27 shows the mean predicted horizontal visibility for all the five sites together. We see that, except HUN, the visibility is very low and ranges from about 40 to 60 m at middle altitudes to about 120-150 m at the edges of the fog layers.

Horizontal visibility in VAN based on empirical and analytical forms
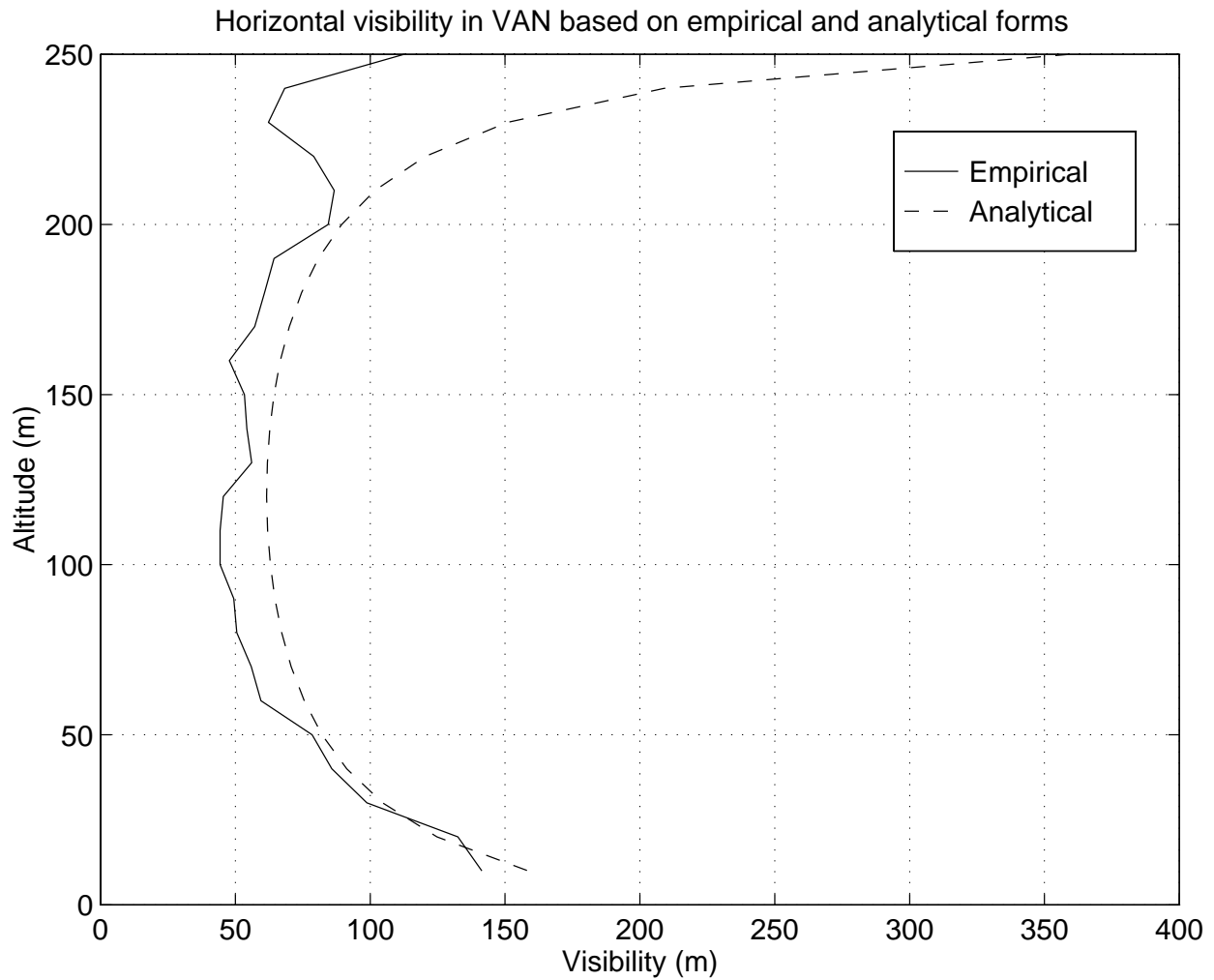
Figure 26. Mean predicted horizontal visibility for VAN by using the empirical relationship based on the measured liquid water content and by using the analytic expression based on the Mie scattering calculations.

Mean predicted horizontal visibility for the five sites
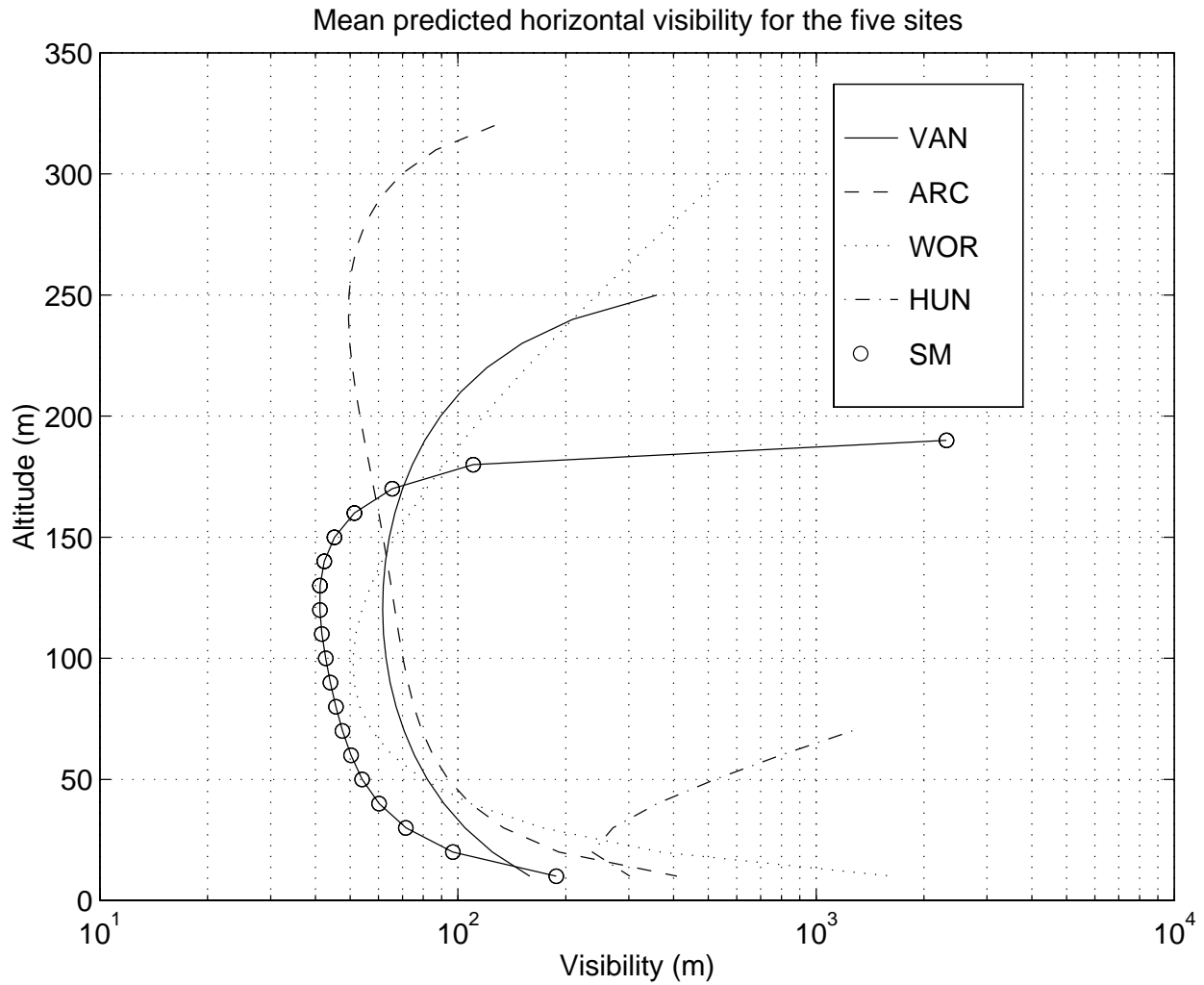
Figure 27. Mean predicted horizontal visibility for the five locations.

A similar approach is used in calculating the vertical visibility. However, since the fog layer is not uniform when looking at the ground, an appropriate integration over the vertical path is needed.

Let z be the current altitude of the aircraft and V the visibility at this point. Applying the definition of visibility (3.14) and (5.7) for the extinction coefficient, we have:

$$\frac{4\pi}{k} \int\limits_{z-V}^{z} d\zeta \int dDn(\zeta, D) f(k, D, n) = 3.912 \tag{5.11}$$

The solution of (5.11) is found numerically..

Figure 28 shows the mean predicted vertical visibility for all the five sites together. We notice that the visibility varies from 50 m to 80 m and the ground is seen at around 70-80 m altitude. At lower altitudes, the visibility, since it exceeds the height level, is depicted as the distance from the ground.
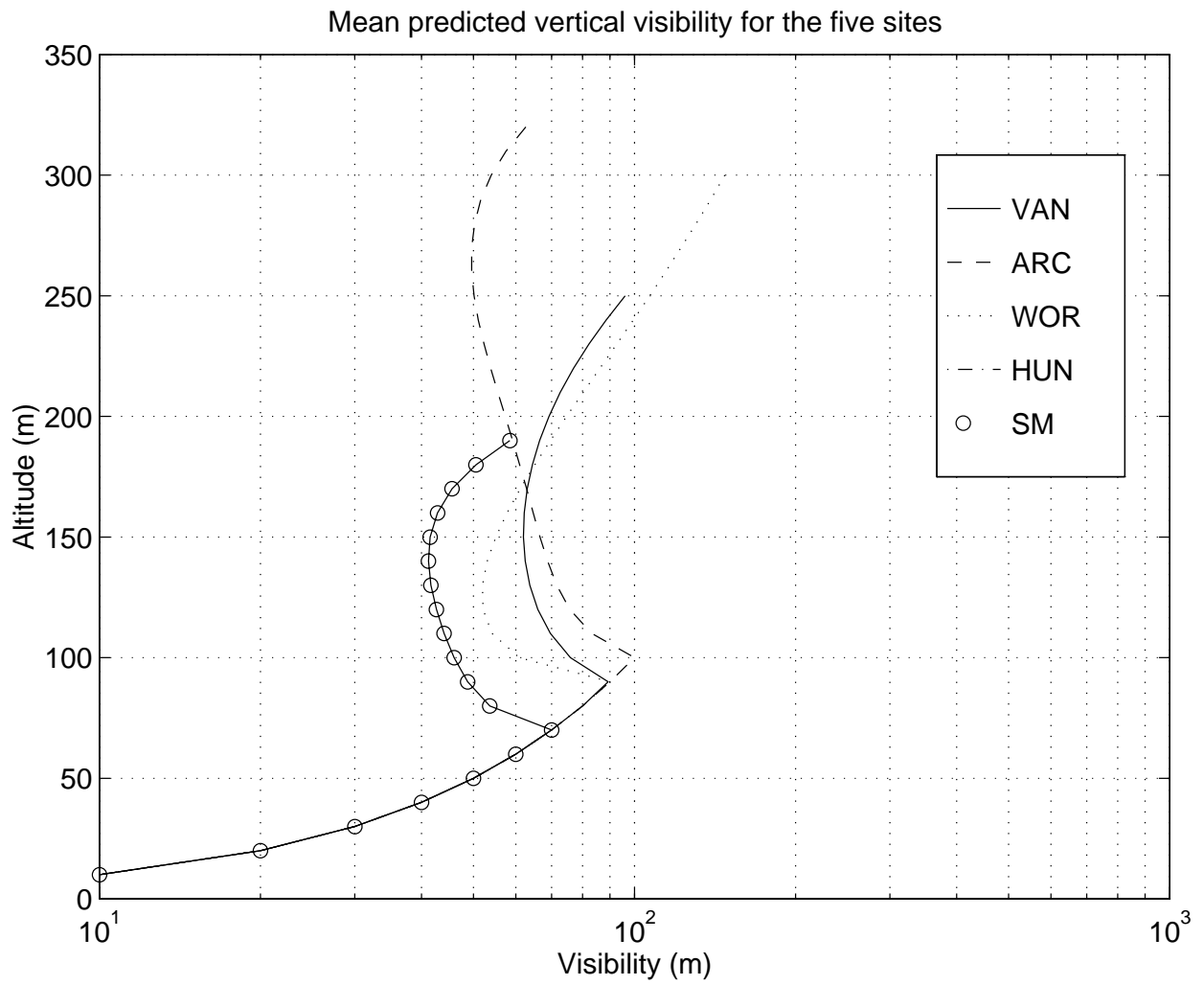
Figure 28. Mean predicted vertical visibility for the five locations.

6. Conclusions

There are many different ways to describe and model the atmospheric aerosols. However, the most widely used to model size distributions are the gamma and the lognormal distribution. These ones are tested and used in this work in modeling the available fog data. The gamma distribution offers an accurate fit to the average data and provides us with easy to handle formulations. More important, it results that the altitude dependence and the size distribution are separable for all the locations. This leads to a size distribution model defined by only one parameter (β). The lognormal distribution seems to better fit the data when a wide range of diameter sizes is included in the analysis. A parameter, which determines the distribution spread, seems to change with temperature changes in a consistent way.

Both the two models predict a linear relationship between the reflectivity factor Z and the liquid water content M. Additionally, the gamma distribution model predicts that the above relationship is altitude independent. A popular empirical law relationship, proposed by Atlas [1], predicts a quadratic dependence and, therefore, contradicts the model estimations. The tests on the data show that, on average, the Z/M ratio is close to constant over the different altitudes. However, other empirical power law relationships have been developed and proposed to more accurately predict Z from M. These relationships are not far from linear.

Atmospheric conditions, such as haze and fog, are found to highly affect the light propagation. Especially fog, and haze to lesser extent, limit visibility considerably and heavily attenuates wave of visible−to−infrared wavelengths. The millimeter waves do not undergo important attenuation except at the higher frequencies (W-band). It is important to mention that despite the accurate fit of the size distribution to the average data, the data exhibit strong variations in density and the resulted standard deviation ranges from 21-97% from site to site. Therefore, there should be expected great discrepancies from the predicted results in practice.

7. References

[1] Atlas D., "Advances in radar meteorology", Adv. in Geophysics, Vol. 10, pp. 317-479, 1964.

[2] Binhua W., "Sea Fog", China Ocean Press, 1985.

[3] Blanco F., P.M. Valdes, "Weather-dependent model of coastal fog attenuation", Optical Engineering, Vol. 31, No.11, pp. 2293-2299, Nov. 1992.

[4] Bohren C.F. and D.R. Huffman, "Absorption and Scattering of Light by Small Particles", Wiley-Interscience, New York, 1983.

[5] Burgess M. A. and R. D. Hayes, "Synthetic Vision, A View in the Fog", Proceedings of the IEEE 11th Digital Avionics System Conference, Seattle, Washington, October 1992.

[6] d'Almeida G.A., P.Koepke, and E.P. Shettle, "Atmospheric Aerosols, Global Climatology and Radiative Characteristics", Ch. 4, A. Deepak Publ., Hampton, VA; 1991.

[7] de Wolf D.A. and L.P. Ligthart, "Multipath effects due to rain at 30-50 GHz frequency communication links", IEEE Trans. Antennas Propagation, AP-41, pp. 1132-1138, 1993.

[8] de Wolf D.A., C. Kontogeorgakis, R.E. Marshall, "Reflectivity and Attenuation at Millimeter to infrared wavelengths for fogs at five locations", paper submitted to the Journal of the Atmospheric Sciences.

[9] Deepak A., "Atmospheric Aerosols. Their Formation, Optical Properties, and Effects", Spectrum Press, 1982.

[10] Deirmendjian D., "Electromagnetic Scattering On Spherical Polydispersions", Elsevier, New York, 1969.

[11] Deirmendjian D., "Use Of Light Scattering Phenomena In Atmospheric Aerosol Monitoring - A Survey", A Radn Note, N-1211-NASA, June 1979.

[12] Doviak R.J., D.S. Zrnic, "Doppler Radar and Weather Observations", Academic Press Inc., 1984.

[13] Friedlander S.K., "Smoke, Dust and Haze -Fundamentals of Aerosol Behavior", J. Wiley & Sons, New York.

[14] Harris D., "The Attenuation of Electromagnetic Waves Due to Atmospheric Fog", International Journal of Infrared and Millimeter Waves, Vol. 16, No. 6, pp. 1091-1108, 1995.

[15] Hobbs, P. V., "Aerosol-Cloud-Climate Interactions", Academic Press Inc., 1993.

[16] Ishimaru A., "Wave Propagation and Scattering in Random Media", Academic Press, New York; 1978.

[17] Jaenicke R., "Physical Aspects of the Atmospheric Aerosol", Aerosols and Their Climatic Effects, H.E. Gerber, A. Deepak, pp. 7-34, 1984.

[18] Junge C.E., "Air Chemistry and Radio Activity", Academic Press, New York; 1963.

[19] Kerr D.E., "Propagation of Short Radio Waves", Dover, New York; 1965.

[20] Marshal R.E., "Optical Visibility in Fog", Research Triangle Institute, 1995.

[21] Marshal R.E., de Wolf D. A., Kontogeorgakis C., "Microwave, Millimeter Wave, IR, and Visible Absorption Along a Glideslope in Fog", RTI Technical Memorandum RTI/4500/46, June 1996.

[22] Marshall R.E, D.A. de Wolf, C. Kontogeorgakis, "Absorption and Reflection in Atmospheric Haze at Visible Through Far Infrared Wavelengths", Technical Memorandum, RTI/4500/046-04S, 1996.

[23] Mason B.J., "The Physics of Clouds", Second Edition, Clarendon Press, 1971.

[24] Mason B. J., "Clouds, Rain, and Rainmaking", Cambridge University Press, 1962.

[25] Mie G., "Beitrage zur Optic trüber Medien speziell kollidaler Matallösungen", Ann. Phys., Vol. 25, pp. 377-445, 1908.

[26] Paluch I.R., C.A. Knight, L.J. Miller, "Cloud Liquid Water and Radar Reflectivity of Nonprecipitating Cumulus Clouds", Journal of the Atmospheric Sciences, Vol. 53, No. 11, pp. 1587-1603, June 1996.

[27] Ray P.S., "Broadband Complex Refractive Indices of Ice and Water", Applied Optics, Vol. 11, No. 8, pp. 1836-1844, Aug. 1972.

[28] Reist P.C., "Aerosol Science and Technology", Second Edition, McGraw-Hill, 1993.

[29] Twomey S., "Atmospheric Aerosols", Elsevier Scientific Publishing Company, 1977.

[30] van de Hulst H.A., "Light Scattering by Small Particles", Wiley & Sons, 1957.

[31] Vasseur H., C.J. Gibbins, "Inference of fog characteristics from attenuation measurements at millimeter and optical wavelengths", Radio Science, Vol. 31, No 5, pp. 1089-1097, Sep.-Oct. 1996.

[32] Whetby K.T., "Modeling of Atmospheric Aerosol Particle Size Distribution", Progress Report (Particle Technology Lab., University of Minnesota, U.S.A., 1975), p.42.

[33] Wu Z.S., K.F. Ren, Y.P. Wang, "10.6 Micron Wave Propagation in Cloud, Fog, and Haze", International Journal of Infrared and Millimeter Waves, Vol. 11, No. 4, pp. 499-504, 1990.

[34] Zak J.A., "Drop size distributions and related properties of fog for five locations measured from aircraft", NASA Contractor Report 4585, (DOT/FAA/CT-94/02), ViGYAN Inc., Hampton, VA., 1994.

[35] Zuev V.E., A.A. Zemlyanov, Yu.D. Kopytin, and A.V. Kuzikovskii, "High-Power Laser Radiation in Atmospheric Aerosols", D. Reidel Publishing Company, 1985.

8. Appendix (Code listing and description)

The following programs / routines are listed :

- average.m

    Matlab code which averages the raw data over the different runs. The input data must be stored in an ASCII file in equal width columns with the following format:

    First column the number of approach, second column the altitude, and the rest columns contain the number of particles in each bin.

- analyze.m

    Matlab code which performs the regression analysis in the raw data and fits a gamma function.

- anlgnm.m

    Matlab code which performs the regression analysis in the raw data and fits a lognormal function.

- fog_att.cc

    C++ code which calculates attenuation, liquid water content, horizontal visibility, vertical visibility, and attenuation coefficient per liquid water content for fog using a function to model the particle size distribution. It includes in separate files the following routines:

    ◊ complex.h

        Defines a class which enables the use of complex variables in c++.

    ◊ mod.f

A function which calculates the module after a division between two integer numbers.

◊   ref_index.f

A function which calculates the real and imaginary part of the refractive index of the water for a given wavelength and temperature. It is based on [27].

◊   bmie.f and fmie.f

A function which returns the imaginary part of the Mie forward scattering coefficient for a given wavelength and set of particle diameters. It is based on [4].

◊   distrib.f

Defines a class that describes the particle size distribution and altitude dependence, and also finds the liquid water content at a given height. This particular one is good for VAN which has a parabolic function to model the altitude dependence.

◊   dist_hun.f

Similar to distrib.f, dist_hun.f defines a class that describes the particle size distribution and altitude dependence, and also finds the liquid water content at a given height. This particular one is good for HUN and WOR which have a gamma function to model the altitude dependence.

```
%--------------------------------------------
%----------------- average.m ----------------
%--------------------------------------------

%The data are passed to the matrix "dat" to be processed.
%The output average data are stored in "z".
%"step" is the height interval.
%"coun" keeps track of the number of the runs for each altitude.

step=10;
sv=min(dat(:,2));
bv=max(dat(:,2));
nol=length(dat(:,1));
noc=length(dat(1,:))-1;
alts=(bv-sv)/step+1;
coun=zeros(1,alts);
z=zeros(alts,noc);

for ii=1:alts,
      for i2=1:nol,
            if dat(i2,2)==bv-(ii-1)*step
                  coun(ii)=coun(ii)+1;
                  for i3=2:noc, z(ii,i3)=z(ii,i3)+dat(i2,i3+1); end;
            end;
      end;
end;

for i1=1:alts,
      z(i1,1)=bv-(i1-1)*step;
      for i2=2:noc,
            z(i1,i2)=z(i1,i2)/coun(i1);
      end;
end;
```

```
%---------------------------------------------
%---------------- analyze.m ----------------
%---------------------------------------------


% ------- Averaging / Calls the routine "average.m" --------

average

% ------- Regression --------

% "beta" stores the beta parameter of the gamma function for each altitude.
% "er" is the error of the approximation for each altitude.
% "g" is the parameter gamma=4 of the gamma function.
% "z2" is the fit distribution.

tmp=zeros(2,noc-1);
z2=z;
beta=zeros(1,alts);
alhpa=zeros(1,alts);
fctr=zeros(1,alts);
er=zeros(1,alts);
g=4;
d1=3.5:3:45.5;
%d2=60:20:100;
diam=d1;
%diam=[d1,d2];
for i1=1:alts,
      nonz=0;
      for i2=2:noc,
            if z(i1,i2)~=0
                  nonz=nonz+1;
                  tmp(1,nonz)=z(i1,i2);
                  tmp(2,nonz)=diam(i2-1);
            end;
      end;
      Ds=tmp(2,1:nonz);
      Bs=g*log(Ds)-log(tmp(1,1:nonz));
      X=[Ds',-ones(nonz,1)];
      res=inv(X'*X)*X'*Bs';
      beta(i1)=res(1);
```

```
        alpha(i1)=exp(res(2));
        z2(i1,2:noc)=alpha(i1)*diam.^g.*exp(-beta(i1)*diam);
        fctr(i1)=sum(z(i1,2:noc))/sum(z2(i1,2:noc));
        alpha(i1)=alpha(i1)*fctr(i1);
        z2(i1,2:noc)=z2(i1,2:noc)*fctr(i1);
        er(i1)=sum((z2(i1,2:noc)-z(i1,2:noc)).^2);
        figure
        plot(diam,z(i1,2:noc));
        hold;
        plot(diam,z2(i1,2:noc),'w--');
end;
```

```
%--------------------------------------------
%---------------- anlognm.m ----------------
%--------------------------------------------


% ------- Averaging / Calls the routine "average.m" --------

average


% ------- Regression --------


% "Dg" stores the Dg parameter of the lognormal function for each altitude.
% "sg" stores the sigma_g parameter of the lognormal function for each
%  altitude.
% "er2" is the error of the approximation for each altitude.
% "zl" is the fit distribution.

tmp=zeros(2,noc-1);
zl=z;
Dg=zeros(1,alts);
sg=zeros(1,alts);
x1=zeros(1,alts);
fctr=zeros(1,alts);
er2=zeros(1,alts);
d1=3.5:3:45.5;
d2=60:20:300;
diam=[d1,d2];
for i1=1:alts,
      nonz=0;
      for i2=2:noc,
            if z(i1,i2)~=0
                  nonz=nonz+1;
                  tmp(1,nonz)=z(i1,i2);
                  tmp(2,nonz)=diam(i2-1);
            end;
      end;
% -------- Lognormal Function --------
      Ds=tmp(2,1:nonz);
      Dg(i1)=sum(z(i1,2:noc).*diam)/sum(z(i1,2:noc));
      bbar=(log(Ds)-log(Dg(i1))).^2/2;
      BB=log(tmp(1,1:nonz)/3)+log(Ds*sqrt(2*pi))-log(sum(z(i1,2:noc)));
```

```matlab
      X=[ones(nonz,1),bbar'];
      res2=inv(X'*X)*X'*BB';
      x1(i1)=exp(exp(-res2(1)));
      x2=exp(1/sqrt(-res2(2)));
      sg(i1)=x2;
      zl(i1,2:noc)=3*sum(z(i1,2:noc))*exp(-(log(diam)-
log(Dg(i1))).^2/(2*(log(sg(i1)))^2))./(log(sg(i1))*diam*sqrt(2*pi));
      er2(i1)=sum((zl(i1,2:noc)-z(i1,2:noc)).^2);

% ------------ Plotting --------------
      figure
      plot(diam,z(i1,2:noc),':');
      hold;
      plot(diam,zl(i1,2:noc),'w-');
end;
```

```
%-----------------------------------------------
%----------------- fog_att.cc ----------------
%-----------------------------------------------

%---------------- variables used: ----------------
% "lamda"    : wavelength
% "T"        : temperature in degrees Celcius
% "xnr"      : real part of the refractive index
% "xni"      : imaginary part of the refractive index
% "fmi"      : imaginary part of the Mie scat. Coef.
% "att"      : attenuation
% "b"        : attenuation coefficient
% "vis_h"    : horizontal visibility
% "vis_v"    : vertical visibility
% "M"        : liquid water content
%---------------------------------------------------

#include <iostream.h>

#include "complex.h"
#include "mod.f"
#include "ref_index.f"

#define num_of_D 100

#include "library/bmie.f"
#include "library/fmie.f"
#include "distrib.f"

int main()
{
      int i,j,NOD=num_of_D;
      double xnr,xni;
      double th=3,s_i=0,b,M;
      double zo=250,z,z2,ex;
      double Dmax=47e-6, Dmin=2e-6;
      double fctr,fct1,step,att,vis_h,vis_v;
      double lamda,T;
      double fmr[num_of_D],fmi[num_of_D],D[num_of_D];
//-------------------------------------------------------------------------
```

```cpp
//------------------- The distributions of the five sites ------------------
//----------------------------------------------------------------------------
      n4 dist(-4.527e+5,-12986,3.14e+6,7.14e+7);                          //VAN
//    n4 dist(-4.917e+5,-0.519,316.77,-6.88e+4,7.11e+6,-1.82e+7);         //ARC
//    n4 dist(-4.573e+5,4.02e+4,2.5126,0.0258);                           //WOR
//    n4 dist(-4.772e+5,5.74e+6,1.3000,0.0660);                           //HUN
//    n4 dist(-4.243e+5,-3.2788,1.151e+3,-1.58e+5,1.11e+7,-2.08e+7);   //SM
//----------------------------------------------------------------------------
      cout<<"\nEnter the wavelength lamda (microns) :";
      cin>>lamda;
      lamda*=1e-6;
      cout<<"\nEnter the temperature (oC) :";
      cin>>T;
      th*=(PI)/180;
      xnr=refre(lamda,T);
      xni=refim(lamda,T);
      cout<<"xnr= "<<xnr<<"      xni= "<<xni<<endl;
//------------- Particle Diameter D integration bin definition ------------
      step=(double) 3.0/NOD;
      for (i=0;i<NOD;i++) {
            ex=-7+step*i;
            D[i]=exp(ex*log(10));
      }
//----------------------------------------------------------------------------
      find_mie(D,xnr,xni,lamda,fmr,fmi);
      for (i=1;i<NOD-1;i++) {
            s_i+=D[i]*fmi[i]*dist.di(D[i]);
      }
      s_i+=0.5*(D[0]*fmi[0]*dist.di(D[0])+D[NOD-1]*fmi[NOD-1]*dist.di(D[NOD-
1]));
      s_i*=(step*lamda/log10(exp(1.0)));
      fct1=20*log10(exp(1));
      cout<<"----------------------------------------------------------------
"<<endl;
      cout<<"   ALT          Attenuation         Liquid          Horizontal
Vertical"<<endl;
      cout<<"   (m)             (dB)            Water          Visibility
Visibility"<<endl;
      cout<<"----------------------------------------------------------------
"<<endl;
```

```
        for (z=zo;z>0;z-=10) {
                fctr=dist.in(z)/(sin(th));
                att=fctr*fct1*s_i;
                b=2*dist.al(z)*s_i;
                vis_h=3.912/b;
                M=dist.lwc(z);
                z2=z;
                do {
                        z2-=0.01;
                        fctr=dist.in(z)-dist.in(z2);
                } while ((fabs(1.0-3.912/(2*fctr*s_i))>0.01)&&(z2>0));
                vis_v=z-z2;
                printf("%6.1f%13.2f%13.4f%15.2f%14.2f\n",z,att,M,vis_h,vis_v);
        }
        cout<<"------------------------------------------------------------
"<<endl;
        printf("Attenuation   per   Liquid   Water   Content   (dB/(km*g/m^3))   :
%8.2f\n\n",4343*b/M);
}
```

```
%---------------------------------------------
%---------------- complex.h ----------------
%---------------------------------------------

#include <math.h>

#define PI 4*atan(1)

class COMPLEX
{
        private:
                double re;
                double im;
        public:
                COMPLEX() {re=0; im=0;}
                COMPLEX(double arg) {re=arg; im=0;}
                COMPLEX(double arg1, double arg2) { re=arg1; im=arg2;}
```

```cpp
                double magn2() { return (re*re+im*im); }
                void show() {
                        if (im<0) cout<<re<<"-j"<<fabs(im);
                                else cout<<re<<"+j"<<im;
                }
          double real() { return (re);}
                double imag() { return (im);}
                COMPLEX operator + (COMPLEX);
                COMPLEX operator - (COMPLEX);
                COMPLEX operator * (COMPLEX);
                COMPLEX operator / (COMPLEX);
};


COMPLEX COMPLEX::operator + (COMPLEX c2)
{
        double re1=re+c2.re;
        double im1=im+c2.im;
        return COMPLEX(re1,im1);
}


COMPLEX COMPLEX::operator - (COMPLEX c2)
{
        double re1=re-c2.re;
        double im1=im-c2.im;
        return COMPLEX(re1,im1);
}


COMPLEX COMPLEX::operator * (COMPLEX c2)
{
        double re1=re*c2.re-im*c2.im;
        double im1=im*c2.re+re*c2.im;
        return COMPLEX(re1,im1);
}
COMPLEX COMPLEX::operator / (COMPLEX c2)
{
        double re1=re*c2.re+im*c2.im;
        double im1=im*c2.re-re*c2.im;
        re1/=c2.magn2();
        im1/=c2.magn2();
        return COMPLEX(re1,im1);
```

```
}

double REAL(COMPLEX c)
{
        return ( c.real());
}

double IMAG(COMPLEX c)
{
        return ( c.imag());
}

COMPLEX CONJG(COMPLEX c)
{
        COMPLEX c1(c.real(),-c.imag());
        return (c1);
}

COMPLEX CMPLX(double arg) {
      COMPLEX c1(arg,0);
      return (c1);
}

COMPLEX CMPLX(double arg1, double arg2) {
      COMPLEX c1(arg1,arg2);
      return (c1);
};
```

```
%---------------------------------------------
%------------------ mod.f ------------------
%---------------------------------------------

int MOD(int n1, int n2)
{
        int nn;
        double x1;
        x1=(double) n1/n2;
```

```
        nn=(int) x1;
        return (n1-nn*n2);
}
```

```
%----------------------------------------------
%---------------- ref_index.f ----------------
%----------------------------------------------
```

ref_index.f

```c
#include <math.h>

#define PI 4*atan(1)

//-------------------------------------------------------------
double find_xnrD(double wvl, double t) {
        double epsinf,epss,xlams,epsrD,epsiD,epsD,xnrD;

        epsinf=5.27137+0.0216474*t-0.00131198*t*t;
        epss=1-4.579e-3*(t-25)+1.19e-5*(t-25)*(t-25);
        epss-=(2.8e-8*(t-25)*(t-25)*(t-25));
        epss*=78.54;
        xlams=3.3836e-6*exp(2513.98/(t+273));
        epsrD=epsinf+(epss-epsinf)/(1+(xlams/wvl)*(xlams/wvl));
        epsiD=(epss-epsinf)*(xlams/wvl)/(1+(xlams/wvl)*(xlams/wvl));
        epsD=sqrt(epsrD*epsrD+epsiD*epsiD);
        xnrD=sqrt((epsD+epsrD)/2);

        return(xnrD);
}
//-------------------------------------------------------------

//---- Real part of refranctive index as a function of lamda ----
double refre(double wvl, double t) {
        int j;
        double xlam0=wvl*1e+6;
        double xnr,xnra,xnrb,xnrD,Tb,tmp1,tmp2;
```

```c
double par[6][3]={{3352.27, 99.914e+4, 15.1963e+4},
            {1639.0, 50.4835e+3, 9246.27},
            {588.24, 84.4697e+4, 10.7615e+5},
            {1639.0, 52340.4, 10399.2},
            {688.24, 345005.0, 259913.0},
            {161.29, 43319.7, 27661.2}};
double a[2]={1.79907, 1.83899};

if (xlam0<=6.0) {
      Tb=0.0001*(t-25)*exp(exp(0.25*log(xlam0/4)));
      xnr=0;
      for (j=0;j<3;j++) {
            tmp1=par[j][0]*par[j][0]-(1e+4/xlam0)*(1e+4/xlam0);
            tmp2=tmp1*tmp1+par[j][2]*(1e+4/xlam0)*(1e+4/xlam0);
            xnr+=(par[j][1]*tmp1/tmp2);
      }
      tmp1=xnr+a[0];
      xnr=(1+Tb)*sqrt(tmp1);
}
if ((xlam0>6.0) && (xlam0<=7.0)) {
      Tb=0.0001*(t-25)*exp(exp(0.25*log(xlam0/4)));
      xnra=0;
      for (j=0;j<3;j++) {
            tmp1=par[j][0]*par[j][0]-(1e+4/xlam0)*(1e+4/xlam0);
            tmp2=tmp1*tmp1+par[j][2]*(1e+4/xlam0)*(1e+4/xlam0);
            xnra+=(par[j][1]*tmp1/tmp2);
      }
      tmp1=xnra+a[0];
      xnra=(1+Tb)*sqrt(tmp1);
      xnrb=0;
      for (j=3;j<6;j++) {
            tmp1=par[j][0]*par[j][0]-(1e+4/xlam0)*(1e+4/xlam0);
            tmp2=tmp1*tmp1+par[j][2]*(1e+4/xlam0)*(1e+4/xlam0);
            xnrb+=(par[j][1]*tmp1/tmp2);
      }
      tmp1=xnrb+a[1];
      xnrb=(1+Tb)*sqrt(tmp1);
      xnr=xnra*(7.0-xlam0)+xnrb*(xlam0-6.0);
}
if ((xlam0>7.0) && (xlam0<=340.0)) {
```

```
            Tb=0.0001*(t-25)*exp(exp(0.25*log(xlam0/4)));
            xnr=0;
            for (j=3;j<6;j++) {
                    tmp1=par[j][0]*par[j][0]-(1e+4/xlam0)*(1e+4/xlam0);
                    tmp2=tmp1*tmp1+par[j][2]*(1e+4/xlam0)*(1e+4/xlam0);
                    xnr+=(par[j][1]*tmp1/tmp2);
            }
            tmp1=xnr+a[1];
            xnr=(1+Tb)*sqrt(tmp1);
        }
    if ((xlam0>340.0) && (xlam0<=1000.0)) {
            xnrD=find_xnrD(wvl,t);
            Tb=0.0001*(t-25)*exp(exp(0.25*log(xlam0/4)));
            xnrb=0;
            for (j=3;j<6;j++) {
                    tmp1=par[j][0]*par[j][0]-(1e+4/xlam0)*(1e+4/xlam0);
                    tmp2=tmp1*tmp1+par[j][2]*(1e+4/xlam0)*(1e+4/xlam0);
                    xnrb+=(par[j][1]*tmp1/tmp2);
            }
            tmp1=xnrb+a[1];
            xnrb=(1+Tb)*sqrt(tmp1);
            xnr=xnrD*((xlam0-340)/660)+xnrb*((1000-xlam0)/660);
        }

        if (xlam0>1000.0) {
            xnrD=find_xnrD(wvl,t);
            xnr=xnrD;
        }


    return (xnr);
}
//-------------------------------------------------------------

//---- Imag.part of refranctive index as a function of lamda ----
double refim(double wvl,double t) {
    double xlam0=wvl*1e+6;
    double PI2=45/PI;
    double epsinf,epss,xlams,epsrD,epsiD,epsD,xniD,xni,s,a;
    double par[18][4]={{2.97, 0.27, 0.025, 2.0},
                {4.95, 0.01, 0.06, 1.0},
```

```
                {2.97, 0.27, 0.04, 2.0},
                {4.95, 0.01, 0.06, 1.0},
                {4.95, 0.01, 0.05, 1.0},
                {6.1, 0.12, 0.08, 2.0},
                {6.1, 0.12, 0.042, 0.6},
                {17.0, 0.39, 0.165, 2.4},
                {62.0, 0.41, 0.22, 1.8},
                {17.0, 0.39, 0.45, 1.3},
                {62.0, 0.41, 0.22, 1.8},
                {300.0, 0.25, 0.40, 2.0},
                {17.0, 0.39, 0.45, 1.3},
                {62.0, 0.41, 0.35, 1.7},
                {300.0, 0.25, 0.40, 2.0},
                {17.0, 0.39, 0.45, 1.3},
                {62.0, 0.41, 0.35, 1.7},
                {300.0, 0.25, 0.47, 3.0}};
     epsinf=5.27137+0.0216474*t-0.00131198*t*t;
     epss=1-4.579e-3*(t-25)+1.19e-5*(t-25)*(t-25);
     epss-=(2.8e-8*(t-25)*(t-25)*(t-25));
     epss*=78.54;
     xlams=3.3836e-6*exp(2513.98/(t+273));
     epsrD=epsinf+(epss-epsinf)/(1+(xlams/wvl)*(xlams/wvl));
     epsiD=(epss-epsinf)*(xlams/wvl)/(1+(xlams/wvl)*(xlams/wvl));
     epsD=sqrt(epsrD*epsrD+epsiD*epsiD);
     xniD=sqrt((epsD-epsrD)/2);
     if (xlam0<=2.97) {
            xni=par[0][1]*exp(-
exp(par[0][3]*log(fabs(log(xlam0/par[0][0])/par[0][2]))));
            xni+=par[1][1]*exp(-
exp(par[1][3]*log(fabs(log(xlam0/par[1][0])/par[1][2]))));
       }
     if ((xlam0>2.97) && (xlam0<=4.95)) {
            xni=par[2][1]*exp(-
exp(par[2][3]*log(fabs(log(xlam0/par[2][0])/par[2][2]))));
                xni+=par[3][1]*exp(-
exp(par[3][3]*log(fabs(log(xlam0/par[3][0])/par[3][2]))));
       }
     if ((xlam0>4.95) && (xlam0<=6.10)) {
                xni=par[4][1]*exp(-
exp(par[4][3]*log(fabs(log(xlam0/par[4][0])/par[4][2]))));
```

```
                        xni+=par[5][1]*exp(-
exp(par[5][3]*log(fabs(log(xlam0/par[5][0])/par[5][2])))));
            }
    if ((xlam0>6.10) && (xlam0<=17.0)) {
                xni=par[6][1]*exp(-
exp(par[6][3]*log(fabs(log(xlam0/par[6][0])/par[6][2])))));
                xni+=par[7][1]*exp(-
exp(par[7][3]*log(fabs(log(xlam0/par[7][0])/par[7][2])))));
            xni+=par[8][1]*exp(-
exp(par[8][3]*log(fabs(log(xlam0/par[8][0])/par[8][2])))));
            }
    if ((xlam0>17.0) && (xlam0<=62.0)) {
                xni=par[9][1]*exp(-
exp(par[9][3]*log(fabs(log(xlam0/par[9][0])/par[9][2])))));
                xni+=par[10][1]*exp(-
exp(par[10][3]*log(fabs(log(xlam0/par[10][0])/par[10][2])))));
                xni+=par[11][1]*exp(-
exp(par[11][3]*log(fabs(log(xlam0/par[11][0])/par[11][2])))));
            }
    if ((xlam0>62.0) && (xlam0<=300.0)) {
                xni=par[12][1]*exp(-
exp(par[12][3]*log(fabs(log(xlam0/par[12][0])/par[12][2])))));
                xni+=par[13][1]*exp(-
exp(par[13][3]*log(fabs(log(xlam0/par[13][0
])/par[13][2])))));
                xni+=par[14][1]*exp(-
exp(par[14][3]*log(fabs(log(xlam0/par[14][0
])/par[14][2])))));
            }
    if ((xlam0>300.0) && (xlam0<=3000.0)) {
                xni=par[15][1]*exp(-
exp(par[15][3]*log(fabs(log(xlam0/par[15][0]
)/par[15][2])))));
                xni+=par[16][1]*exp(-
exp(par[16][3]*log(fabs(log(xlam0/par[16][0
])/par[16][2])))));
                xni+=par[17][1]*exp(-
exp(par[17][3]*log(fabs(log(xlam0/par[17][0
])/par[17][2])))));
            }
```

```
        xni+=xniD;
        if (xlam0>3000) {
            s=12.5664e+8;
            a=-16.8129/(t+273)+0.0609265;
            epsrD=(epss-epsinf)*(1+sin(a*PI2/2)*exp((1-a)*log(xlams/wvl)));
            epsrD/=(1+2*sin(a*PI2/2)*exp((1-a)*log(xlams/wvl))+exp(2*(1-
a)*log(xlams/wvl)));
            epsrD+=epsinf;
            epsiD=(epss-epsinf)*cos(a*PI2/2)*exp((1-a)*log(xlams/wvl));
            epsiD/=(1+2*sin(a*PI2/2)*exp((1-a)*log(xlams/wvl))+exp(2*(1-
a)*log(xlams/wvl)));
            epsiD+=s*wvl*1e+2/18.8496e+10;
            epsD=sqrt(epsrD*epsrD+epsiD*epsiD);
            xni=sqrt((epsD-epsrD)/2);
        }
        return (xni);
}
//---------------------------------------------------------------
```

```
void bhmie(double x, COMPLEX refrel, int nang, COMPLEX* s1, COMPLEX* s2)
{
        int j,jj,n,nn,nmx;
        double p,t,rn;
        double ymod,xstop,nstop,dang;
        double psi0,psi1,psi,dn,dx,fn;
        double qext,qsca,qback;
        double chi,chi0,chi1,apsi,apsi0,apsi1;
        double theta[100], amu[100], pi[100], tau[100], pi0[100], pi1[100];
        double *integ;
        COMPLEX y,tmp1,tmp2,tmp3;
        COMPLEX d[30000],xi,xi0,xi1,an,bn;

        dx=x;
```

```
        tmp1=CMPLX(x);
        y=tmp1*refrel;
        xstop=2+x+4*exp(log(x)/3);
        nstop=xstop;
        ymod=sqrt(y.magn2());
        nmx=(int) (xstop>ymod) ? xstop:ymod;
        nmx+=15;
        dang=(double) 0.5*(PI)/(nang-1);
        for (j=1;j<=nang;j++) {
                theta[j]=(double) (j-1)*dang;
                amu[j]=cos(theta[j]);
        }
        nn=nmx-1;
        for (n=1;n<=nn;n++) {
                rn=nmx-n+1;
                tmp1=CMPLX(double (rn));
                tmp1=tmp1/y;
                tmp2=CMPLX(1.);
                d[nmx-n]=tmp1-(tmp2/(d[nmx-n+1]+tmp1));
        }
        for (j=1;j<=nang;j++) {
                pi0[j]=0;
                pi1[j]=1;
        }
        nn=2*nang-1;
        for (j=1;j<=nn;j++) {
                s1[j]=CMPLX(0);
                s2[j]=CMPLX(0);
        }

// Riccati-Bessel

        psi0=cos(dx);
        psi1=sin(dx);
        chi0=-sin(x);
        chi1=cos(x);
        apsi0=psi0;
        apsi1=psi1;
        xi0=CMPLX(apsi0,-chi0);
        xi1=CMPLX(apsi1,-chi1);
```

```
      qsca=0;
      n=1;
do {
      dn=n;
      rn=n;
      fn=(double) (2*rn+1)/(rn*(rn+1));
      psi=(2*dn-1)*psi1/dx-psi0;
      apsi=psi;
      chi=(double) (2*rn-1)*chi1/x-chi0;
      xi=CMPLX(apsi,-chi);
      tmp1=CMPLX(double (rn)/x);
      tmp2=d[n]/refrel+tmp1;
      an=CMPLX(tmp2.real()*apsi-apsi1,tmp2.imag()*apsi);
      an=an/(tmp2*xi-xi1);
      tmp2=refrel*d[n]+tmp1;
      bn=CMPLX(tmp2.real()*apsi-apsi1,tmp2.imag()*apsi);
      bn=bn/(tmp2*xi-xi1);
      qsca+=(double) (2*rn+1)*(an.magn2()+bn.magn2());
      for (j=1;j<=nang;j++) {
            jj=2*nang-j;
            pi[j]=pi1[j];
            tau[j]=(double) rn*amu[j]*pi[j]-(rn+1)*pi0[j];
            p=(MOD(n,2)==0) ? -1.0:1.0;
            tmp1=CMPLX(pi[j]);
            tmp2=CMPLX(tau[j]);
            tmp3=CMPLX(fn);
            s1[j]=s1[j]+tmp3*(an*tmp1+bn*tmp2);
            t=(MOD(n,2)==0) ? 1.0:-1.0;
            s2[j]=s2[j]+tmp3*(an*tmp2+bn*tmp1);
            if (j!=jj) {
                  tmp1=CMPLX(pi[j]*p);
                  tmp2=CMPLX(tau[j]*t);
                  s1[jj]=s1[jj]+tmp3*(an*tmp1+bn*tmp2);
                  s2[jj]=s2[jj]+tmp3*(an*tmp2+bn*tmp1);
            }
      }
      psi0=psi1;
      psi1=psi;
      apsi1=psi1;
      chi0=chi1;
```

```
        chi1=chi;
        xi1=CMPLX(apsi1,-chi1);
        n=n+1;
        rn=n;
        for (j=1;j<=nang;j++) {
             pi1[j]=(double) ((2*rn-1)/(rn-1))*amu[j]*pi[j];
             pi1[j]=(double) pi1[j]-rn*pi0[j]/(rn-1);
             pi0[j]=pi[j];
        }
    }  while (n-1-nstop<0);
    qsca*=2/(x*x);
    qext=(4/(x*x))*s1[1].real();
    qback=(4/(x*x))*s1[2*nang-1].magn2();
}
```

```
%------------------------------------------------
%------------------ fmie.f ------------------
%------------------------------------------------


void find_mie(double *rad, double refre, double refim, double wavel, double
*sflr, double *sfli)
{
int count=1;
      int k,j,nang,nan;
      double refmed=1.0,waven,freq,ang,angr;
      double aj,pol,radlog;
      double s11nor,s11,s12,s33,s34;
      double x,qext,qsca,qback,dang;
      COMPLEX s1[200],s2[200],refrel,sflux1;
      COMPLEX tmp1,tmp2;

      tmp1=CMPLX(refre,refim);
      tmp2=CMPLX(refmed);
      refrel=tmp1/tmp2;
      waven=2*(PI)/wavel;
      freq=(double) 299792458/wavel;
      for (k=0;k<num_of_D;k++) {
```

```
            x=(PI)*rad[k]*refmed/wavel;
            nang=33;
            dang=0.5*(PI)/(nang-1);
            bhmie(x,refrel,nang,s1,s2);
            s11nor=0.5*(s2[1].magn2()+s1[1].magn2());
            nan=2*nang-1;
            for (j=1;j<=1;j++) {
                    aj=j;
                    s11=0.5*(s2[j].magn2()+s1[j].magn2());
                    s12=0.5*(s2[j].magn2()-s1[j].magn2());
                    pol=-s12/s11;
                    s33=REAL(s2[j]*CONJG(s1[j]))/s11;
                    s34=IMAG(s2[j]*CONJG(s1[j]))/s11;
                    s11=s11/s11nor;
                    tmp1=CMPLX(waven);
                    sflux1=s1[j]/tmp1;
                    ang=(double) dang*(aj-1)*180/(PI);
                    angr=(double) ang*(PI)/180;
                    tmp1=CMPLX(cos(angr));
                    sflux1=sflux1*tmp1;
                    sfli[k]=sflux1.real();
                    sflr[k]=-sflux1.imag();
            }
        }
}




%---------------------------------------------
%----------------- distrib.f -----------------
%---------------------------------------------

class n4
{
      private:
            double q,beta;
            double a,b,c;
```

```
        public:
                n4(double arg2,double arg3,double arg4,double arg5) {
                        beta=arg2; a=arg3; b=arg4; c=arg5;
                        q=pow(-beta,5)/24.0;
                }
                double di(double d) {
                        return (q*exp(4*log(d))*exp(beta*d));
                }
                double al(double z) {
                        return (a*z*z+b*z+c);
                }
                double in(double z) {
                        return (a*z*z*z/3+b*z*z/2+c*z);
                }
                double lwc(double z) {
                        return ((PI)*5040.0*q*1e+6*(a*z*z+b*z+c)/(6*pow(-beta,8)));
                }
};




%---------------------------------------------
%---------------- dist_hun.f ----------------
%---------------------------------------------

class n4
{
      private:
                double q,beta;
                double a,b,c;
      public:
                n4(double arg2,double arg3,double arg4,double arg5) {
                        beta=arg2; a=arg3; b=arg4; c=arg5;
                        q=pow(-beta,5)/24.0;
                }
                double di(double d) {
                        return (q*exp(4*log(d))*exp(beta*d));
                }
                double al(double z) {
```

```
                return (a*exp(b*log(z)-c*z));
        }
        double in(double z) {
                double f=0,tmp,g;
                int n,i;
                n=1;
                g=(c*z)/(b+1+n);
                tmp=g;
                do {
                        n++;
                        g*=(c*z)/(b+1+n);
                        tmp+=g;
                } while (g>1e-5);
                f=tmp+1;
                return                          (a*exp((b+1)*log(c*z)-
c*z)*f/(exp((b+1)*log(c))*(b+1)));
        }
        double lwc(double z) {
                return   ((PI)*5040.0*q*1e+6*(a*exp(b*log(z)-c*z))/(6*pow(-
beta,8)));
        }
};
```

Vita

Christos Kontogeorgakis, son of Vassilios Kontogeorgakis and Georgia Dimopoulou, was born on April 13, 1970, in Almyros, Greece. He received his Diploma degree in Electrical Engineering in March, 1994, from the Aristotle University of Thessaloniki, Greece. Prior to continuing in higher education, he did his military service in the Greek Air Force from July 1994 to July 1995. Then, he was accepted in the graduate program in the Department of Electrical Engineering at Virginia Polytechnic Institute and State University. He began his studies towards the degree of Master of Science as a Research Assistant for Dr. David A. de Wolf in August 1995. He completed his program, specializing in electromagnetic wave propagation through atmospheric aerosols, in May 9, 1997.

Currently, he is pursuing his Ph.D. degree in Electrical Engineering as a team member of MPRG (Mobile and Portable Radio Research Group) at Virginia Tech.

Christos Kontogeorgakis

May, 1997.